Estuarine, Coastal and Shelf Science 316 (2025) 109183

Contents lists available at ScienceDirect

Estuarine, Coastal and Shelf Science

journal homepage: www.elsevier.com/locate/ecss

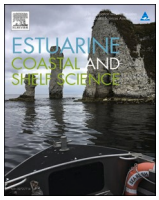

Larval dispersal dynamics of *Maja squinado* in the Northwestern Mediterranean: a biophysical modeling approach

C. Barrier [a,*], T. Beneteau [a], M.-C. Raffalli [a,b], N. Barrier [c], C. Lett [c], V. Pasqualini [a,b], E.D.H. Durieux [a,b,**]

[a] Université de Corse, UMR CNRS 6134 Sciences pour l'Environnement, Corte, France
[b] Université de Corse, UAR CNRS 3514 Stella Mare, Biguglia, France
[c] MARBEC, Université de Montpellier, CNRS, Ifremer, IRD, Sète, France

ARTICLE INFO

Keywords:
Maja squinado
Larval dispersal
Mediterranean sea
Biophysical models
Regional connectivity

ABSTRACT

The Mediterranean spinous spider crab, *Maja squinado* (Herbst, 1788), is a prized crustacean exploited by Mediterranean coastal fisheries, contributing to local economies and culinary traditions. While stock declines have been reported in some regions, other areas continue to sustain fishing activities, albeit under pressure. Understanding the species' demography is therefore essential for effective future management. To investigate the larval dispersal dynamics of *M. squinado* in the Mediterranean, a biophysical model was developed, incorporating biological and ecological data such as larval duration and spawning habitats. The tool Ichthyop, designed to study ichthyoplankton dynamics, was employed to perform simulations spanning the period from 2010 to 2020. These simulations were analyzed in the context of global surface water warming trends, yielding maps that illustrated trajectory density, system connectivity, and variations in larval density and dispersal distance over time. The comparative analysis of various scenarios revealed the significant impact of environmental variations on larval connectivity. Specifically, the Tunisia-Sardinia-Corsica complex exhibited strong connectivity, while the Balearic Islands appeared isolated due to the species' short pelagic larval duration (PLD). The findings highlight the utility of biophysical models in hypothesizing population declines in isolated areas and underscore the necessity of employing diverse modeling approaches at multiple spatial and temporal resolutions. Kernel density estimation (KDE) maps were selected to analyze and visualize the observed simulation scenarios. The results emphasize the importance of considering these changes, particularly the synergies between environmental and biological parameters that influence larval dispersal and connectivity in this species. Such approaches could enhance future conservation and management strategies by accounting for the complex interactions driving population dynamics within the context of a changing Mediterranean ecosystem.

1. Introduction

The Mediterranean Sea is a biodiversity hotspot, representing 4–18% of global marine species (Bianchi and Morri, 2000). This reservoir has been under increasing pressure for several decades due to habitat degradation, marine and atmospheric pollution, invasive species, and climate change. Fishing is a major activity in the Mediterranean Sea, with catches reaching 1.19 million tons in total in 2020. The majority of fisheries are industrial, with an annual catch of 1 million tons. Yet, this activity represents only 17% of the total number of boats, with the remaining 83% engaged in artisanal fishing (FAO, 2020). The lack of regulation of artisanal vessels, illicit fishing practices, the discard of unwanted catch, and the overfishing of fish stocks have collectively led to the overexploitation of marine resources and an irreversible decline in fish stocks (Carlson et al., 2016; Zaimen et al., 2021). Besides, the majority of specific fish stocks have not yet been assessed, making it difficult for political decision-makers to apply and establish regulations (Marengo et al., 2016). Among the marine species affected by these anthropogenic pressures, the Mediterranean spinous spider crab (*Maja squinado*) has gained particular attention due to its ecological and economic importance. Indeed, a sa locally important fishing resource, the Mediterranean spinous spider crab *Maja squinado* (Herbst, 1788) has

* Corresponding author.
** Corresponding author. Université de Corse, UMR CNRS 6134 Sciences pour l'Environnement, Corte, France.
E-mail addresses: BARRIER_C@univ-corse.fr (C. Barrier), durieux_e@univ-corse.fr (E.D.H. Durieux).

https://doi.org/10.1016/j.ecss.2025.109183
Received 28 June 2024; Received in revised form 4 February 2025; Accepted 5 February 2025
Available online 6 February 2025

experienced a significant decline in its population in recent years, likely due to overexploitation (Abelló et al., 2014; Durán et al., 2013; Martín et al., 2012; Rotllant et al., 2014).

In areas such as the Balearic Islands or the Columbretes Islands, the species appears to be nearly extinct for approximately a decade, prompting research and reintroduction initiatives (Garcia, 2007; Torres et al., 2013). Given this decrease in stocks, *Maja squinado* is internationally recognized as a species of ecological interest within the United Nations Environment Programme's Action Plan for the Mediterranean (UNEP/MAP). Additionally, it was included as a protected species in the Bern Convention for the Conservation of European Wildlife and Natural Habitats and was added to Appendix III of the Barcelona Convention in 2009. In France, the IUCN has not yet concluded on the species' status, however regional decrees are already applied in order to limit and regulate catches by recreational fishing. In Corsica, populations still support small-scale fisheries (Bousquet et al., 2022); however, a notable decline in CPUEs (Catches per Unit Effort) has been observed in recent years (Marengo et al., 2023). To better understand the factors contributing to the decline of *Maja squinado* populations, it is essential to examine its life history traits, reproductive biology, and dispersal mechanisms, which play critical roles in the species' persistence and connectivity.

Maja squinado, a member of the Majidae family, was initially described as inhabiting both the Atlantic and the Mediterranean Sea. In 1998, Neumann proposed a distinction between *Maja squinado* and *Maja brachydactyla* (Balss, 1922) based on morphological characteristics identified by Balss in 1922, with the respective distribution areas assigned to the Mediterranean and the Atlantic (Neumann, 1998). This differentiation was further supported by a genetic study that analyzed mitochondrial gene variations in Atlantic (*Maja brachydactyla*) and Mediterranean (*Maja squinado* and *Maja crispata*) spider crab populations (Sotelo et al., 2008). Given that a substantial portion of research on *Maja squinado* has, in reality, focused on the Atlantic species *Maja brachydactyla*, our knowledge of *Maja squinado* in the Mediterranean remains relatively limited and varies depending on geographic region and author. Gualtieri et al. (2013) for example, in their study along the Corsican coast of the Mediterranean Sea using wireless acoustic sensors, observed that spider crabs migrate to deeper waters in winter and return to coastal areas during spring and summer. Their findings also indicate that these crabs are stationary within their habitat at night but actively move during daylight hours. Similarly, Rotllant et al. (2015) reported that adult specimens, predominantly ovigerous females (those carrying eggs), were captured along the Catalan coast (Spain) in April. Gravid females ascend to shallower waters in summer to spawn, while males typically remain in deeper habitats. These females possess a spermatheca, enabling them to spawn multiple times from winter matings. The number of egg clutches and larvae varies according to authors, geographical areas, and water temperatures. Each female produces approximately three clutches of 30,000 to 200,000 larvae (Calado et al., 2013; Durán et al., 2012). Gravid females incubate the eggs under their abdomen before releasing the larvae at the zoea I stage, which then progress through three stages: zoea I (ZI), zoea II (ZII), and megalopa. *Maja squinado* eggs and larvae are carried by currents and drift in the environment to complete their lifecycle. This process involves biological and physical mechanisms that facilitate the movement of larvae from breeding to recruitment sites (Begon et al., 2005).

Larval transport in species with multiphasic life cycles has historically been considered to be heavily influenced by current patterns (J. Power, 1984). However, biotic factors such as migratory abilities driven by diel or ontogenetic cycles, as well as swimming and orientation capacities, can also play a significant role in these dispersion processes (Adams et al., 2012; Gary et al., 2020). Broadly speaking, exchanges across various spatial scales are deemed critical for understanding connectivity and the dynamics of marine metapopulations (Pineda et al., 2007). Crustacean larvae, particularly decapods, have not been observed engaging in active swimming. Although vertical migration has not been thoroughly investigated in *Maja squinado*, studies on other crustacean species have demonstrated that larvae are capable of diel vertical migrations, shifting between depths in response to day-night cycles (Anger et al., 2015; Ospina-Alvarez et al., 2018).

Understanding the population dynamics of *Maja squinado* is crucial for developing effective management and conservation strategies. Although biophysical models are not often used for population dynamics, they are frequently employed to investigate pelagic larval dispersal and connectivity (Swearer et al., 2019). By integrating biophysical modeling, we can gain insights into the species' larval stages, aiding in the prediction of dispersal patterns and connectivity, which are essential for informed management and conservation efforts. This approach offers numerous benefits for predicting and visualising the dynamics of population dispersal and for hypothesizing species vulnerabilities. For example, it can highlight isolated habitats or a lack of connectivity between populations, which are critical for effective conservation strategies (Jahnke and Jonsson, 2022; Lett et al., 2010). Individual-based models (IBMs) are designed to include detailed information about the life history traits of species for which researchers intend to model spatial and/or temporal dynamics (DeAngelis and Mooij, 2005). Each individual in the model is defined by a set of state variables and behaviours, which are determined according to available information on the species and the model's desired level of precision. These include geographical location, physiological traits, and certain behavioural traits such as reproduction and habitat selection. In a biophysical model, the trajectories of particles representing larvae are influenced by ocean currents and other environmental factors. By incorporating larval behaviours and physiological processes, the model becomes more precise, allowing for refined predictions that align more closely with other scientific approaches studying the species of interest.

In many Brachyura species, larval dispersal and migration are shaped by dominant ocean currents, as well as seasonal changes, water temperature, and food availability (Anger, 1991; Bryars and Havenhand, 2006; Epifanio & Garvine, 2001b; Anger et al., 2015). In the Mediterranean Sea, particularly in its northwestern region, recent research (Margirier et al., 2020) has highlighted an annual increase in temperature of +0.06 °C and salinity of +0.012. Furthermore, a significant shift was observed in 2014, particularly in the properties of the offshore Ligurian Levantine Intermediate Water (LIW).This warming trend, which aligns with broader global patterns (Pastor et al., 2020; Yin et al., 2018), underscores the importance of investigating how environmental shifts may affect species such as *Maja squinado* and whether global change signals, such as rising temperatures, could play a role in the synergy of biotic and abiotic factors influencing larval dispersal and connectivity processes in species like the one studied in the present research. In light of these dynamics, a critical knowledge gap remains regarding the influence of environmental changes on larval dispersal and connectivity. Addressing this gap is crucial for predicting population persistence and informing conservation strategies.

Thus, the current observation is that despite having experienced a substantial decline in certain regions, such as the Balearic Islands, *Maja squinado* remains fished elsewhere—most notably around Corsica—although its IUCN status is currently non-evaluated. Because its ecology and population dynamics are not fully understood, reliable projections for the species' future distribution remain challenging. To address these challenges, this study adopts a biophysical modeling approach to explore the larval dispersal and connectivity of *Maja squinado* in the Northwestern Mediterranean. By doing so, we aim to provide critical insights into how environmental and biological factors shape the species' spatial dynamics. Recognizing the significance of larval dispersal for population persistence, this study harnesses a biophysical modeling approach to explore the dispersal and connectivity of *M. squinado* larvae across the Northwestern Mediterranean from 2010 to 2020. Specifically, we aim (i) to offer an initial prediction of larval dispersal routes over an extended time frame, (ii) to evaluate connectivity patterns among key habitats identified in the literature, and (iii) to

integrate scenarios that account for recent increases in sea surface temperature. By combining spatial and temporal analyses, we seek to shed light on how global warming signals may influence the connectivity of this vulnerable species and to provide a basis for more informed management strategies.

2. Material and methods

2.1. Mediterranean's surface circulation

The Mediterranean Sea is divided into two main basins, the Western and Eastern, separated by the Sicily-Tunisia Strait. The Western Basin extends from the Alboran Sea to the Tyrrhenian Sea, with the Atlantic Ocean connected to it via the Strait of Gibraltar. The Eastern Basin extends from the Adriatic to the Levantine Sea, including the Ionian and Libyan Seas. The Mediterranean Sea's intricate surface circulation, influenced by its segmented geography and complex seabed, predominantly exhibits anticyclonic movement. Fresh Atlantic waters enter the Mediterranean through the Strait of Gibraltar, increasing in density due to evaporation before exiting, typically taking 50–100 years to circulate. Surface currents are influenced by wind and topography, forming stable gyres and up to 1-km-wide eddies. However, some areas exhibit instabilities over time (Millot and Taupier-Letage, 2005; Pinardi et al., 2015) (Fig. 1A).

Surface currents in the northwestern Mediterranean are primarily influenced by thermohaline circulation, with cyclonic currents observed near the continental slopes. Notable currents include the Liguro-Provençal-Catalan Current, which flows in an east-to-west direction, and various gyres such as the Gulf of Lion Gyre and the Northern Tyrrhenian Gyre, which exhibit distinct circulatory patterns. Furthermore, the Tyrrhenian Sea's connectivity with the Corsican and Sardinian shores is characterised by the presence of various currents and gyres, which collectively contribute to the formation of a dynamic marine environment (Pinardi et al., 2015) (Fig. 1B).

2.2. Hydrodynamical models

The simulations for this study were performed using two hydrodynamic models. The first one, MEDSEA_MULTIYEAR_PHY_006_004 (MedMFC), was used to carry out simulations encompassing the entirety of particle release polygons representing larvae in the Western Mediterranean. This model, which presents a daily temporal resolution, integrates a hydrodynamic model contributed by the Nucleus for European Modelling of the Ocean (NEMO). It is further enhanced by a variational data assimilation approach known as OceanVAR, which processes vertical profiles of temperature and salinity, along with satellite-derived sea level anomaly data. The dataset includes a comprehensive reanalysis segment, as well as an interim segment that extends from the end of the reanalysis to one month prior to the current date. The model operates on a finely calibrated horizontal grid with a resolution of 1/24°, equivalent to approximately 4–5 km (Escudier et al., 2021). A second hydrodynamic model, MARS3DMed, was employed for focused analyses and to attempt observing phenomena at a finer scale. This model, derived from the MARS3D (Model for Application at Regional Scales 3D) code and developed by Ifremer, has a temporal resolution of 3 h, a horizontal resolution of about 1.2 km, and 60 vertical levels using a generalized sigma coordinate system on an Arakawa-C grid, extending from the seabed to the surface, and is adapted for fine graphical resolutions (Arakawa & Lamb, 1977; Lazure and Dumas, 2008).

The regional configuration of the MARS3D model been validated against observational data. Specifically, studies by Pairaud et al. (2011) and Gatti and Pairaud (2010). Similarly, the MedMFC model has undergone validations achieved through comparisons with in situ

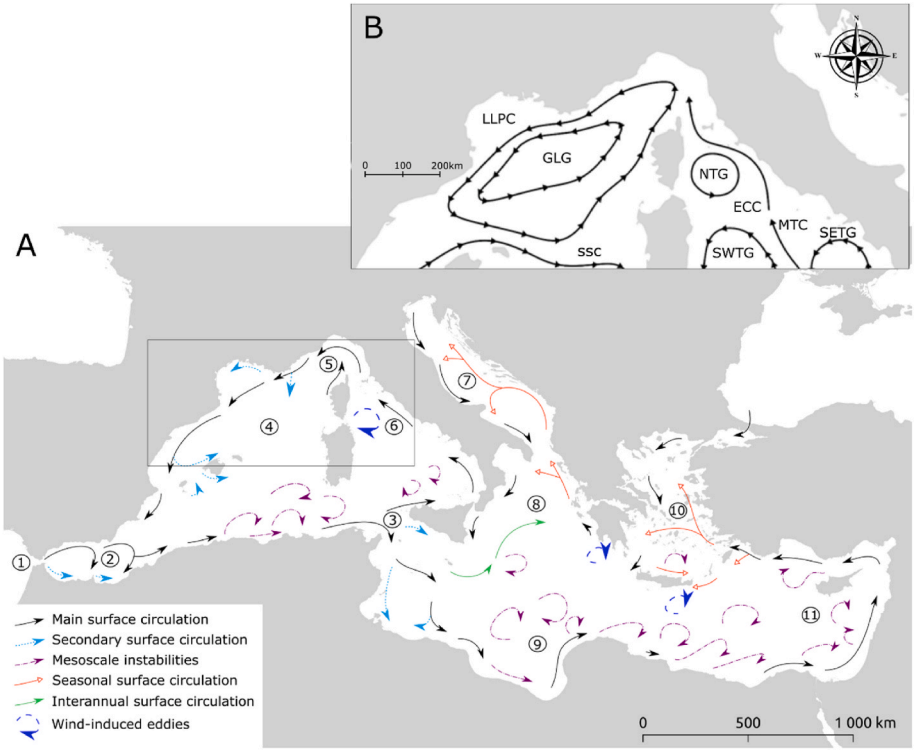

Fig. 1. Map of the general circulation currents in the Mediterranean (A), covering all basins (adapted from Millot and Taupier-Letage, 2005). 1: Strait of Gibraltar, 2: Alboran Sea, 3: Sicilia-Tunisia Strait, 4: Algero-Provençal Basin, 5: Ligurian Sea, 6: Tyrrhenian Sea, 7: Adriatic Sea, 8: Ionian Sea, 9: Libyan Sea, 10: Aegean Sea, 11: Levantine Sea. **Focus on the Northwestern Mediterranean Sea (B)** adapted from the study by Pinardi et al. (2015). LPCC: Liguro-Provençal-Catalan Current, GLG: Gulf of Lion Gyre, NTG: Northern Tyrrhenian Gyre, ECC: Eastern Corsica Current, SSC: Southern Sardinia Current, MTC: Middle Tyrrhenian Current, and SETG: South-Eastern Tyrrhenian Gyre.

observations, including Conductivity-Temperature-Depth (CTD) profiles, ARGO floats, and satellite-derived data such as altimetry and sea surface temperature (SST). The evaluation was further supported by the calculation of root mean square differences (RMSD), confirming the system's capability to accurately represent the physical state of the Mediterranean Sea (Escudier et al., 2021).

2.3. Model parametrisation in the Lagrangian transport tool

The larval dispersal model employed is Ichthyop v.3.3.16, an offline Java-based Lagrangian tool (Lett et al., 2008). This biophysical model has been widely applied in marine ecology (Rojas-Araos et al., 2024; Flores-Valiente et al., 2023) and physical oceanography (Al-Qattan et al., 2023; de Mello et al., 2023), allowing for the integration of both physical and biological factors in the study of ichthyoplankton dynamics. Ichthyop tracks the movement of water masses or particles based on outputs from ocean circulation models such as ROMS, MARS, NEMO, or SYMPHONIE (Imzilen et al., 2023). Particle trajectories are computed using a fourth-order Runge-Kutta method with a constant time step to ensure compliance with the Courant-Friedrichs-Lewy (CFL) condition. For MARS3DMed, a time step of 720 s was used, while a step of 2880 s was applied for MedMFC outputs. Particle positions were recorded at regular intervals (every 60th and 15th time step, respectively) to capture their trajectories every 12 h.

Horizontal diffusion parameters followed Ichthyop's default configuration (Peliz et al., 2007), with a dissipation rate of 10^{-9} m^2/s^3. Vertical migration was based on diel cycles, reflecting the depth and timing of sunrise and sunset (Table 1). Notably, buoyancy was incorporated into the vertical velocity calculations, with particle density set to 0.9 g/cm^3. This value, supported by findings from Epifanio and Garvine (2001), ensures that particles remain in the upper layers of the water column, as observed in this crustacean larval studies. Furthermore, vertical migration during the day-night cycle was modeled as a critical aspect of the larval life cycle, with depths averaging 30 m during the day and 1 m at night (Anger et al., 2015; Ospina-Alvarez et al., 2018). While horizontal migration was not included, early larval stages (zoeae) were limited to vertical swimming, transitioning to walking and feeding appendages at later stages (megalopa and juvenile stages).

Particle release parameters were designed to simulate larval dispersal during the spawning period of *Maja squinado* in the Western Mediterranean, with documented spawning data from Corsica and Catalonia (Calado et al., 2013; Durán et al., 2012; Rotllant et al., 2014). Because precise measurements of release timing are lacking in the literature, particle release dates were evenly distributed across the identified spawning period, ensuring representative coverage. Each simulation year included eight release events (April 15–May 31), consistent with the literature (Table 1).

For MedMFC, 50,000 particles were released per event, amounting to 400,000 particles per simulation or 4,400,000 particles over the 11-year study, distributed evenly across 36 zones. In MARS3DMed, a proportional approach was adopted, with 31,250 particles released per event, yielding 250,000 particles per simulation or 2,750,000 over the study period, evenly allocated across 23 polygons in the Northwestern Mediterranean. These values adhere to recommendations from Simons et al. (2013), which establish guidelines on the particle numbers needed for robust modeling.

The dispersal period was capped at 20 days, with larval competency for settlement starting at 17 days, representing the onset of the juvenile stage (Durán et al., 2012; Rotllant et al., 2014). Particle retention was modeled such that particles located within recruitment zones after 17 days were immobilized, while those remaining outside recruitment zones after 20 days were classified as unsuccessful. Finally, particles interacted with physical boundaries through rebound behavior, overcoming these barriers with forces calibrated to ichthyoplankton dynamics.

Table 1
Biological parameters of the simulations applied to the dispersion of *Maja squinado*.

Parameter	Value	Reference
Pelagic larval duration (PLD)	20 days	Durán et al. (2012)
Release date (per year)	April 15 - Start of the laying period. April 22 - One week after the start. April 29 - Two weeks after the start. May 6 - Three weeks after the start. May 13 - Four weeks after the start. May 20 - Five weeks after the start. May 27 - Six weeks after the start. May 31 - End of the laying period.	
Particles number	MedMFC: 50000 particles were released on each release day (8 days in total), amounting to 400000 particles per simulation. This equates to 4400000 particles over the 11-year study period, distributed evenly across 36 zones. MARS3DMed: in order to maintain proportional relationships, 31250 particles were released each day of the release period (8 days in total), resulting in a total of 250000 particles per simulation, or 2750000 particles over the 11-year study period, distributed evenly across 23 polygons in the Northwestern Mediterranean.	
Release depth	0–50m for MedMFC model	Gualtieri et al. (2013)
Release polygons	See Fig. 2 for geographical localization: 1: MA1, 2: SP2, 3: SP5, 4: SP6, 5: SP7, 6: SP8, 7: SP9, 8: FR2, 9: FR3, 10: FR-I, 11: CAPi, 12: NWCO The following codes correspond to the polygon numbers: 13: WCO, 14: SWCO, 15: SCO, 16: SECO, 17: NECO, 18: IT3, 19: IT4, 20: NSA, 21: NWSA, 22: SWSA, 23: SSA, 24: SESA, 25. The following abbreviations are used in this document: NESA, 26: IT7, 27: IT8, 28: IT9, 29: IT10, 30: SIC1, 31: SIC2, 32: USTi, 33: SIC3, 34: TUN, 35: AL3, 36: MA-AL.	Rotllant et al., (2014), Guerao and Rotllant (2010), Guerao et al., (2016), Seytre et al., (2013), Modena et al., (2001); Durán et al., (2012) and grey littérature.
Ideal habitat for recruitment polygons	See Fig. 3 for geographical localization: 1:MA1, 2:ALB, 3: SP1, 4:SP2, 5:SP3, 6:SP4, 7: SP5, 8:SP6, 9:COLUI, 10:SP7, 11:BA2, 12:BA1, 13:BA3, 14: BA4, 15:BA8, 16:BA5, 17: SP8, 18:BA7, 19:SP9, 20:BA6, 21:SP-FR, 22:FR1, 23:FR2, 24:FR3, 25:FR4, 26:FR-I, 27: IT1, 28:CAPi, 29:NWCO, 30: WCO, 31:SWCO, 32:SCO, 33: SECO, 34:NECO, 35:IT2, 36: IT3, 37:PIAI, 38:IT4, 39:IT5, 40:NSA, 41:NWSA, 42:SWSA, 43:SSA, 44:SESA, 45:NESA, 46:IT6, 47:IT7, 48:IT8, 49:	Rotllant et al., (2014), Guerao and Rotllant (2010), Guerao et al., (2016), Seytre et al., (2013), Modena et al., (2001); Durán et al., (2012) and grey littérature.

(*continued on next page*)

Table 1 (*continued*)

Parameter	Value	Reference
	IT9, 50:IT10, 51:SIC1, 52: EOLI, 53:SIC2, 54:USTi, 55: SIC3, 56:TUN, 57:ALTUN, 58: GALI, 59:AL4, 60:AL3, 61: AL2, 62:AL1, 63:MA-AL.	
Minimum retention age	17 days	Rotllant et al. (2014)
Buoyancy	0.9 g/cm^3	Epifanio and Garvine (2001a)
Vertical migration depth	day: 30m – night: 1m	Ospina-Alvarez et al. (2018)
Coastal particles behaviour	Bouncing	

2.4. Delimitation of release and recruitment sites

The 36 zones used for the release of particles were designed based on the documented presence of *Maja squinado* in the literature (Rotllant et al., 2014; Guerao and Rotllant, 2010; Guerao et al., 2016; Seytre et al., 2013; Modena et al., 2001; Durán et al., 2012; Rotllant et al., 2015; Angeletti et al., 2014; Gualtieri et al., 2013; Durán et al., 2013; Calado et al., 2013; Sotelo et al., 2008; Vignoli et al., 2004; Mura and Corda, 2011; Pipitone and Arculeo, 2003, Fig. 2). Additionally, based on these bibliographic references, the 63 recruitment zones were parameterized by identifying habitats favorable for the settlement of larvae and juveniles, all within a realistic bathymetric range (<50 m; Fig. 3).

2.5. Environmental trends visualization and data analysis

The Ichthyop simulation outputs are files in NetCDF format, which were analyzed using R (version 4.0.4; R Core Team, 2021) and Python (version 3.11) scripts. Density maps of particle trajectories were generated for the entire simulation period (2010–2020). Trajectory densities were calculated in several steps: first, the final positions of particles were extracted from the simulation outputs. The coordinates (longitude and latitude) of these particles were used to create spatial line objects, subsequently converted into spatial vector objects. These vectors were rasterized onto a background grid map, where each raster cell represented the cumulative number of particle trajectories passing through it. This process quantified the particle density spatially by summing the trajectories in each grid cell. To evaluate relative variability, a coefficient of variation (CV) was computed for the density maps. The CV facilitated comparisons of relative trajectory variability between years or periods, accounting for differences in absolute densities. Connectivity matrices between release zones and recruitment zones, as well as local retention leading to potential self-recruitment at each site. On connectivity matrices, a Gini coefficient (Hixon and Jones, 2005) was also displayed to assess disparities between years and sites. The Gini coefficient is a synthetic indicator used to measure the level of inequality for a given variable within a specific population. It ranges from 0 (perfect equality) to 1 (extreme inequality). The closer the index is to 1, the more unequal the contribution of years to the observed average connectivity percentages; conversely, the closer it is to 0, the more equal the contribution. This method enables the observation of relationships with varying stability over the study period through a color gradient displayed in the matrices.

The sea surface temperature data extracted from the Copernicus Marine Environment Monitoring Service (CMEMS) satellite product over the western Mediterranean Sea revealed a temperature increase trend of 0.034 ± 0.002 °C per year, with a 95% confidence interval (Appendix Figure A1). To analyze spatial trends and focus on the last decade, data from the MedMFC model were examined at all grid points in the Western Mediterranean (with a particular focus on the study

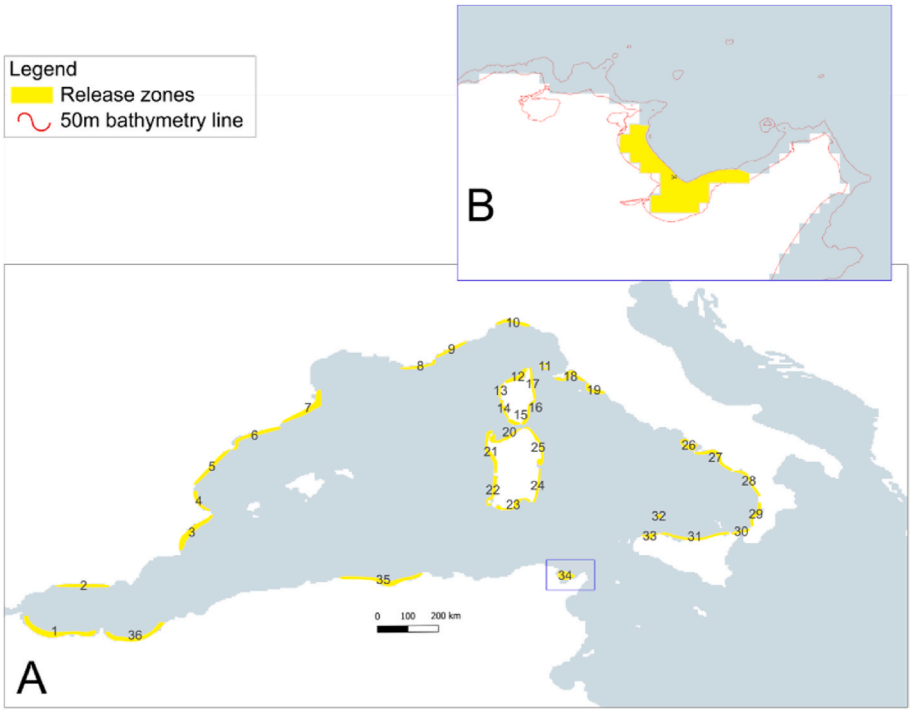

1	MA1	Strait of Gibraltar (Morocco)
2	SP2	Andalusia (Spain)
3	SP5	Almería / Murcia (Spain)
4	SP6	Valencia / Alicante (Spain)
5	SP7	Southern Catalonia (Spain)
6	SP8	Catalonia (Spain)
7	SP9	Gulf of Lion (France–Spain border)
8	FR2	Provence–Côte d'Azur (France)
9	FR3	Liguria (France)
10	FR-I	Liguria (Italy)
11	CAPi	Capraia Island (Italy)
12	NWCO	Northwest Corsica (France)
13	WCO	West Corsica (France)
14	SWCO	Southwest Corsica (France)
15	SCO	Southwest Corsica–Strait of Bonifacio (France)
16	SECO	Southeast Corsica–Strait of Bonifacio (France)
17	NECO	Northeast Corsica (France)
18	IT3	North Tyrrhenian Sea Coast (Italy)
19	IT4	North Tyrrhenian Sea Coast (Italy)
20	NSA	Northeast Sardinia (Italy)
21	NWSA	Northwest Sardinia (Italy)
22	SWSA	Southwest Sardinia (Italy)
23	SSA	South Sardinia (Italy)
24	SESA	Southeast Sardinia (Italy)
25	NESA	Northeast Sardinia (Italy)
26	IT7	South Tyrrhenian Sea Coast (Italy)
27	IT8	South Tyrrhenian Sea Coast (Italy)
28	IT9	South Tyrrhenian Sea Coast (Italy)
29	IT10	South Tyrrhenian Sea Coast (Italy)
30	SIC1	Strait of Messina, Sicily (Italy)
31	SIC2	Northeast Sicily (Italy)
32	USTi	Ustica Island, Sicily (Italy)
33	SIC3	Northwest Sicily (Italy)
34	TUN	Gulf of Tunis (Tunisia)
35	AL3	Algerian Coast (Algeria)
36	MA-AL	Algerian–Moroccan Border

Fig. 2. Diagram of the 36 release polygons (yellow, panel A), shown along the coastlines. The polygons were positioned as close as possible to the 50 m bathymetric contour. The table to the right of the map provides a correspondence between zone codes and their indices, covering various zones and islands. The polygons were created in QGIS, adhering to the spatial resolution of the hydrodynamic model. A closer view of Zone 34 (code TUN for the Gulf of Tunis, panel B) illustrates in detail—rather than schematically—how the polygons are drawn to remain within the 0–50 m bathymetric range (panel B, red line), while staying inside the model's data domain (blue color) without encroaching upon areas lacking data (white areas). (For interpretation of the references to color in this figure legend, the reader is referred to the Web version of this article.)

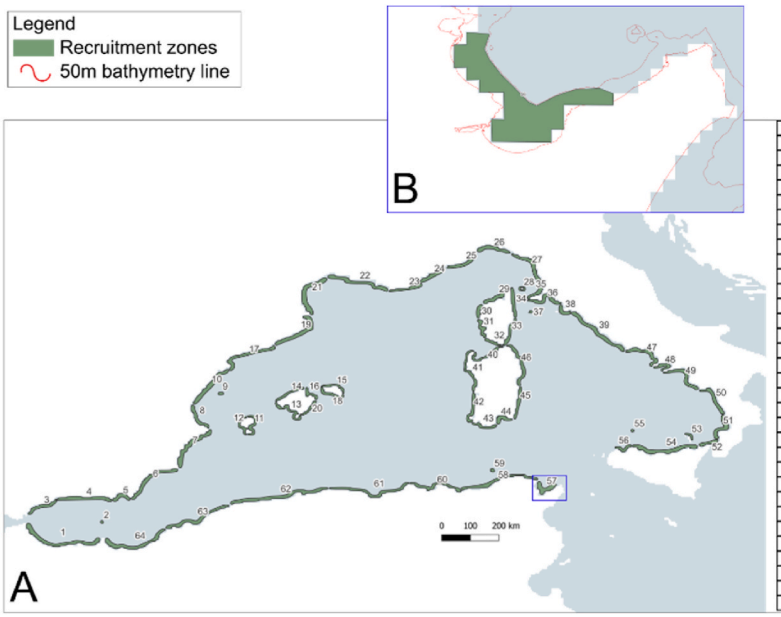

1	MA1	Strait of Gibraltar (Morocco)	34	NECO	Northeast Corsica (France)
2	ALB	Île d'Alboran (Spain)	35	IT2	Tuscan Archipelago 1 (Italy)
3	SP1	Strait of Gibraltar (Spain)	36	IT3	Tuscan Archipelago 1 (Italy)
4	SP2	Andalusia 1 (Spain)	37	PIAI	Pianosa Island (Italy)
5	SP3	Andalusia 2 (Spain)	38	IT4	North Tyrrhenian Sea Coast 1 (Italy)
6	SP4	Andalusia 3 (Spain)	39	IT5	North Tyrrhenian Sea Coast 2 (Italy)
7	SP5	Almería / Murcia (Spain)	40	NSA	Northeast Sardinia (Italy)
8	SP6	Valencia / Alicante (Spain)	41	NWSA	Northwest Sardinia (Italy)
9	COLUI	Columbretes Islands (Spain)	42	SWSA	Southwest Sardinia (Italy)
10	SP7	Southern Catalonia (Spain)	43	SSA	South Sardinia (Italy)
11	BA2	Balearic Islands 1 (Spain)	44	SESA	Southeast Sardinia (Italy)
12	BA1	Balearic Islands 2 (Spain)	45	NESA	Northeast Sardinia (Italy)
13	BA3	Balearic Islands 3 (Spain)	46	IT6	South Tyrrhenian Sea Coast 1 (Italy)
14	BA4	Balearic Islands 4 (Spain)	47	IT7	South Tyrrhenian Sea Coast 2 (Italy)
15	BA8	Balearic Islands 5 (Spain)	48	IT8	South Tyrrhenian Sea Coast 3 (Italy)
16	BA5	Balearic Islands 6 (Spain)	49	IT9	South Tyrrhenian Sea Coast 4 (Italy)
17	SP8	Catalonia (Spain)	50	IT10	South Tyrrhenian Sea Coast 5 (Italy)
18	BA7	Balearic Islands 7 (Spain)	51	SIC1	Strait of Messina, Sicily (Italy)
19	SP9	France–Spain border	52	EOLI	Aeolian Islands (Italy)
20	BA6	Balearic Islands 8 (Spain)	53	SIC2	Northeast Sicily (Italy)
21	SP-FR	Gulf of Lion 1 (France)	54	USTI	Ustica Island, Sicily (Italy)
22	FR1	Gulf of Lion 2 (France)	55	SIC3	Northwest Sicily (Italy)
23	FR2	Provence–Côte d'Azur (France)	56	TUN	Gulf of Tunis (Tunisia)
24	FR3	Liguria (France)	57	ALTUN	Algerian–Tunisian border
25	FR4	France-Italy border	58	GALI	Galite Islands (Tunisia)
26	FR-I	Liguria 1 (Italy)	59	AL4	Algerian Coast 1 (Algeria)
27	IT1	Liguria 2 (Italy)	60	AL3	Algerian Coast 2 (Algeria)
28	CAPI	Capraia Island (Italy)	61	AL2	Algerian Coast 3 (Algeria)
29	NWCO	Northwest Corsica (France)	62	AL1	Algerian Coast 4 (Algeria)
30	WCO	West Corsica (France)	63	MA-AL	Algerian–Moroccan border
31	SWCO	Southwest Corsica (France)			
32	SCO	Southwest Corsica–Strait of Bonifacio (France)			
33	SECO	Southeast Corsica–Strait of Bonifacio (France)			

Fig. 3. Diagram of the 63 recruitment polygons (green, panel A), shown along the coastlines. The polygons were positioned as close as possible to the 50 m bathymetric contour. The table to the right of the map provides a correspondence between zone codes and their indices, covering various zones and islands. A closer view of zone 57 (code TUN for the Gulf of Tunis, panel B) illustrates in detail how the polygons are drawn to remain within the 0–50 m bathymetric range (panel B, red line), while staying inside the model's data domain (blue color) without encroaching upon areas lacking data (white areas). (For interpretation of the references to color in this figure legend, the reader is referred to the Web version of this article.)

area), providing a more spatially detailed view of regional temperature variations. Linear regression was applied to compute a linear temperature trend for each grid point, with a color gradient ranging from blue (indicating a decrease in temperature) to red (indicating an increase). These trends were visualized on a map, and a comprehensive discussion of these findings is provided in the appendix section. To further understand the ecological implications of these temperature changes, we investigated the potential impact of environmental shifts on the dispersal of *M. squinado* by dividing the simulation outputs into two groups: 2010–2014 and 2015–2019. This grouping allowed for a comparison of periods with differing average temperatures while ensuring an equal number of simulations per scenario. A general visualization was performed using kernel density estimates (KDEs). The KDE calculation relies on a symmetric function centered on each data point, with the Gaussian kernel (normal distribution) being the most commonly used. The bandwidth parameter determines the degree of smoothing: smaller bandwidths result in more detailed estimates, whereas larger bandwidths produce smoother estimates. For particle position simulations modeling larval dispersal, KDEs enable the estimation of spatial density at different times, facilitating the visualization of areas with high particle concentrations and the detection of differences between the two scenarios. The kernels represent the spatial distributions of larval positions at the final step of the simulations, highlighting the areas where larval densities are highest.

Finally, a focused analysis was conducted on two specific zones—SP9, located at the France-Spain border, and SWCO, in southwest Corsica—to examine the distribution of distances traveled and directions followed from release to recruitment. These zones were selected because they exhibit both noteworthy similarities and distinct differences, underscoring their relevance for studying *M. squinado* population connectivity. SP9 demonstrates limited connectivity to the recruitment areas of the Balearic Islands, whereas SWCO is integrated into a broader larval connectivity network involving Tunisia, Sardinia, Corsica, and the Ligurian Sea. Notably, while *M. squinado* has been completely extirpated from areas such as the Balearic Islands, as documented in the literature, the species persists—though in decline—in Corsica and neighboring coastlines, where it is still exploited.

Distances traveled by the larvae were calculated using the Haversine formula, which accurately accounts for the Earth's curvature by computing great-circle distances between points. The resulting plots illustrate the distribution and density of traveled distances, enabling a comparison of particle densities from spawning areas across two climatic scenarios: pre- and post-warming periods in the Western Mediterranean. Additionally, wind rose diagrams were constructed to analyze the predominant orientations of particle dispersal upon their arrival at recruitment zones. Orientation angles were calculated by averaging the angles of individual trajectory segments, with weights proportional to the distances traveled within each segment. These complementary visualizations provide a detailed depiction of both the spatial and directional patterns of larval dispersal in response to environmental changes.

Finally, statistical analyses were conducted on the datasets derived from the simulation predictions for each year and scenario, with a specific focus on the distances traveled by particles that successfully reached a recruitment zone. These analyses began with a normality assessment using the Shapiro-Wilk test. When data deviated from normality, the non-parametric Kruskal-Wallis test was applied to identify significant differences in traveled distances within each zone, comparing the two periods in the context of environmental changes. When significant differences were detected, post hoc Dunn's tests were performed to pinpoint the specific years in which these differences occurred.

3. Results

3.1. Investigating temporal and spatial variability of dispersion pathways over the entire temporal period (2010–2020)

Maps of particle density's coefficient of variation (CV) computed over the entire study period and domain covered by the MedMFC model highlight the principal simulated routes and their temporal variability for larvae transported from spawning to recruitment zones (Fig. 4). We note a continuity in the simulated larval dispersal pattern of *Maja squinado* between the North and South around Corsica and Sardinia,

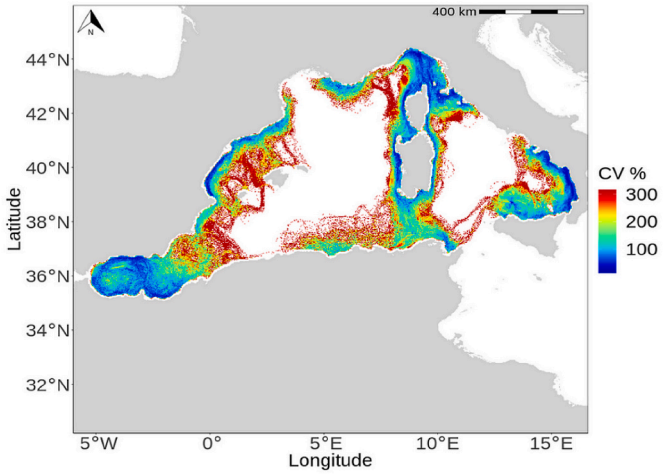

Fig. 4. Density map of particles that successfully reach a recruitment zone averaged for the period 2010 to 2020, based on simulations carried out with the MedMFC model in the Western Mediterranean. The interannual variability of these trajectories is expressed by a coefficient of variation (CV).

with low CV values, indicating that this pattern is recurrent along the study period. In contrast, other areas, such as the Balearic Islands, have less connection with the coastlines, or at least less regularly along the study period. Lastly, the Alboran Sea emerges as a significant exchange hub for larvae along its various coastlines, yet it has limited connection with the rest of the Western Mediterranean.

The MARS3DMed model (Fig. 5) reveals that trajectories with low coefficients of variation primarily connect nearby coastal areas, at times forming interconnected sets over the course of the eleven considered years. This is exemplified by the routes appearing on both sides along Corsica and Sardinia. The broader geographic window used with MedMFC allows for the identification of routes in the southern Western Mediterranean, particularly in the Alboran Sea, which is minimally or not connected to the rest of the sub-basins. Furthermore, the Balearic Islands are geographically isolated, although a few trajectories (with very high coefficients of variation) exhibit weak connectivity to the Spanish coastlines over the studied period. The southern coastlines of Sardinia are connected with the Tunisian coastlines on a regular basis over time. This creates a group with probable larval exchanges between Tunisia, Sardinia, and then Corsica moving northward.

The Gulf of Lion is also a site of significant exchanges, with distinct routes emerging: one arriving from the east and another departing towards the west. Notwithstanding the high CV (panel C of Fig. 5) of these routes, they play a pivotal role in regional connectivity. In the easternmost part of the Western Mediterranean, there is also a coastal route along the Sicilian-Italian coastline with minimal connectivity to the rest of the basin, with the exception of a few trajectories (with high CV) connecting to the Tunisian coasts.

The connectivity matrix (Fig. 6) was organized in a manner consistent with the Mediterranean sub-basins. The maximum connectivity values of approximately 9% were obtained in the cluster Italy-Sicily-Tunisia, between the IT8 and IT9 (south Tyrrhenian Sea Coast). In the Alboran Sea, we observe regular connectivity relationships (as indicated by a low Gini index) and remarkably high local retention values for MA1

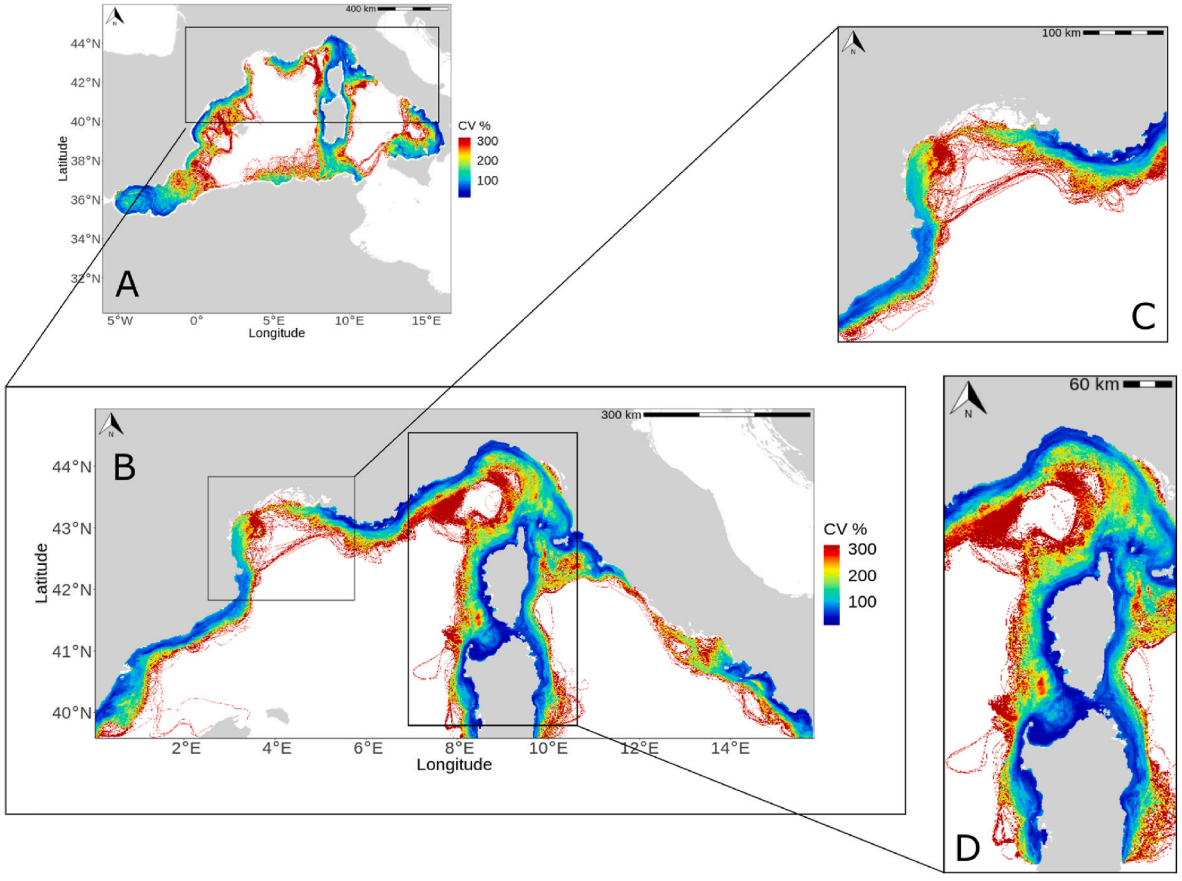

Fig. 5. Trajectory densities for the entire period from 2010 to 2020 generated using two hydrodynamic models with different geographical windows and foci. A: Simulations carried out with the MedMFC model in the western Mediterranean. B: Simulations carried out with the MARS3DMed model in the north-western Mediterranean, allowing finer resolution focuses in C (Gulf of Lion) and D (Sardinia-Corsica ensemble). The variability of the trajectories over time is expressed by the coefficients of variation (CVs).

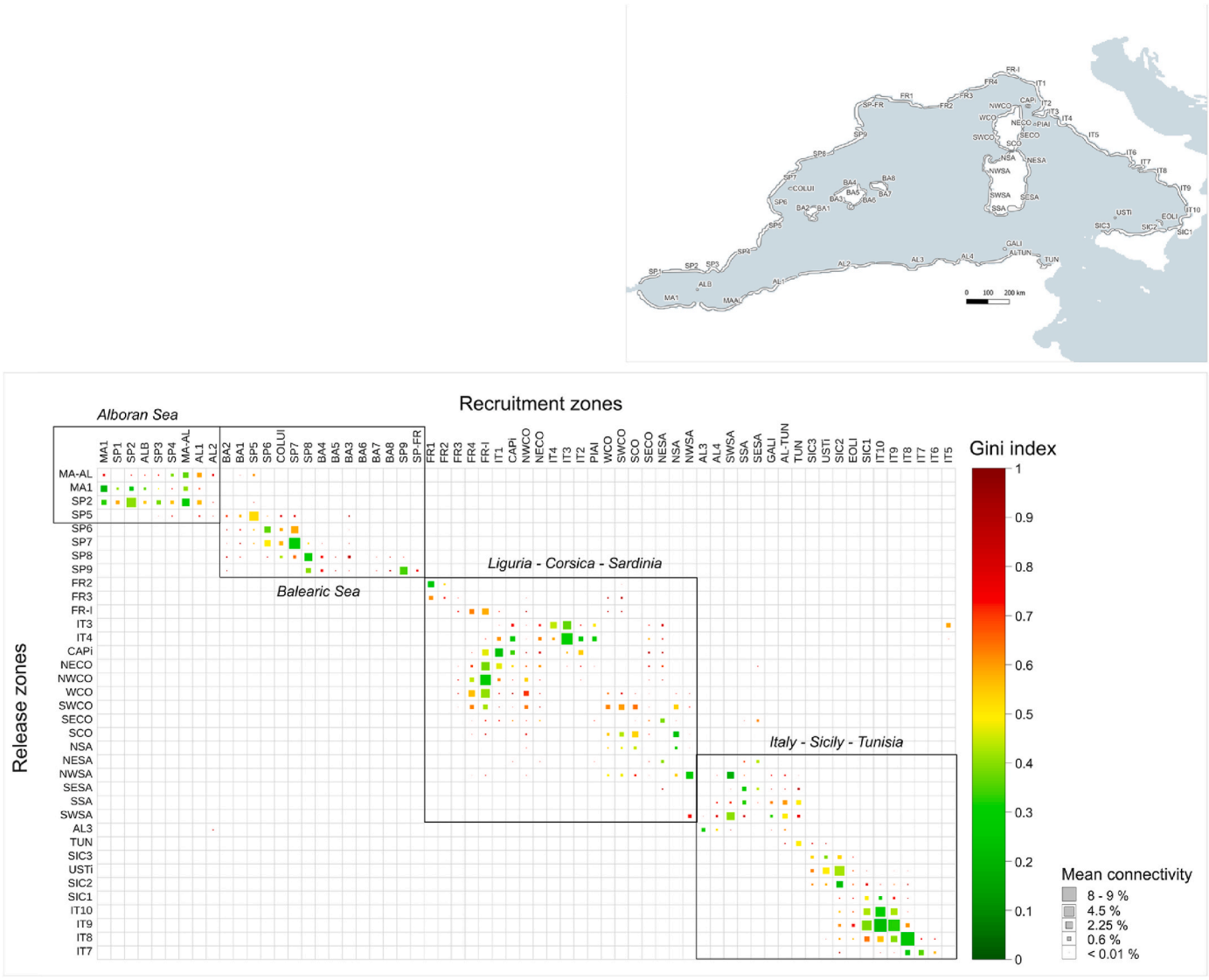

Fig. 6. The connectivity matrix was developed based on simulations conducted using the MedMFC model in the Western Mediterranean region, covering the period from 2010 to 2020. The release zones are represented on the vertical axis, while the recruitment zones are shown on the horizontal axis. Color gradients indicate the Gini index values, and sub-basins representing clusters of zones are outlined. The accompanying map provides spatial context for the zones within the basin. (For interpretation of the references to color in this figure legend, the reader is referred to the Web version of this article.)

(Strait of Gibraltar, Morocco) and SP2 (Andalusia coast, Spain). In the Balearic Sea, the most notable features are the high local retention within SP7, SP8 (Catalonia coasts, Spain), and SP9 (France–Spain border), all with low Gini indices, thus illustrating relatively consistent exchanges over time. The Balearic Islands (BA1 to BA9) are connected by small amounts of particles, with Gini indices higher than 0.5. The Corsica-Sardinia area and the coasts of the Ligurian Sea have connections close to the maximum of obtained connectivity values (e.g., IT3, the Tuscan Archipelago) with IT4 (north Tyrrhenian Sea coast), NWCO (northwest Corsica) with FR-I (Ligurian coast), WCO (west Corsica) with FR-I (Ligurian coast) with low Gini indices.

Local retention values in Corsica can reach notable percentages, as observed in the FR-I zone (France–Italy border) with a mean connectivity ranging between 2% and 3%. However, the Gini index, ranging between 0.5 and 0.7, indicates a process that does not appear consistent over the entire temporal period according to simulation predictions. Similarly, a Gini index close to 0.5 is observed for the mean connectivity between the Corsican zones (e.g., NWCO, WCO, SCO) and the Sardinian zones (e.g., NWSA, SSA). Thus, in general, we observe relatively regular exchanges between Corsica, Sardinia, and the Ligurian coasts. Finally, the last remarkable group is that of the Italian, Sicilian, and Tunisian coasts, where some of the highest connectivity levels are observed between the zones IT7 to IT10 (South Tyrrhenian Sea coasts), with strong local retention within each of these zones as well, and low Gini indices. The Tunisian zone (TUN, Gulf of Tunis) is connected to the Sardinian zones (e.g., SWSA, SSA) and the Sicilian zones (e.g., SIC1, SIC2, USTi) are connected to both the Aeolian Islands (EOLI) and the Italian zones south of the Tyrrhenian Sea (e.g., IT8, IT9).

3.2. *Analysis of trends in light of global change signals in the western Mediterranean*

3.2.1. *Warming signals and comparison of larval recruitment kernels*

The kernel density estimates (KDE) maps for the periods 2010–2014 and 2015–2019 were produced by dividing the simulation outputs into two distinct datasets. This approach aimed to identify discernible differences in larval kernel densities and their geographic distributions at a macroscopic scale at the end of their larval dispersal. The first map (Fig. 7A) represents the 2010–2014 scenario and illustrates the larval density across the geographic space during this period, calculated using

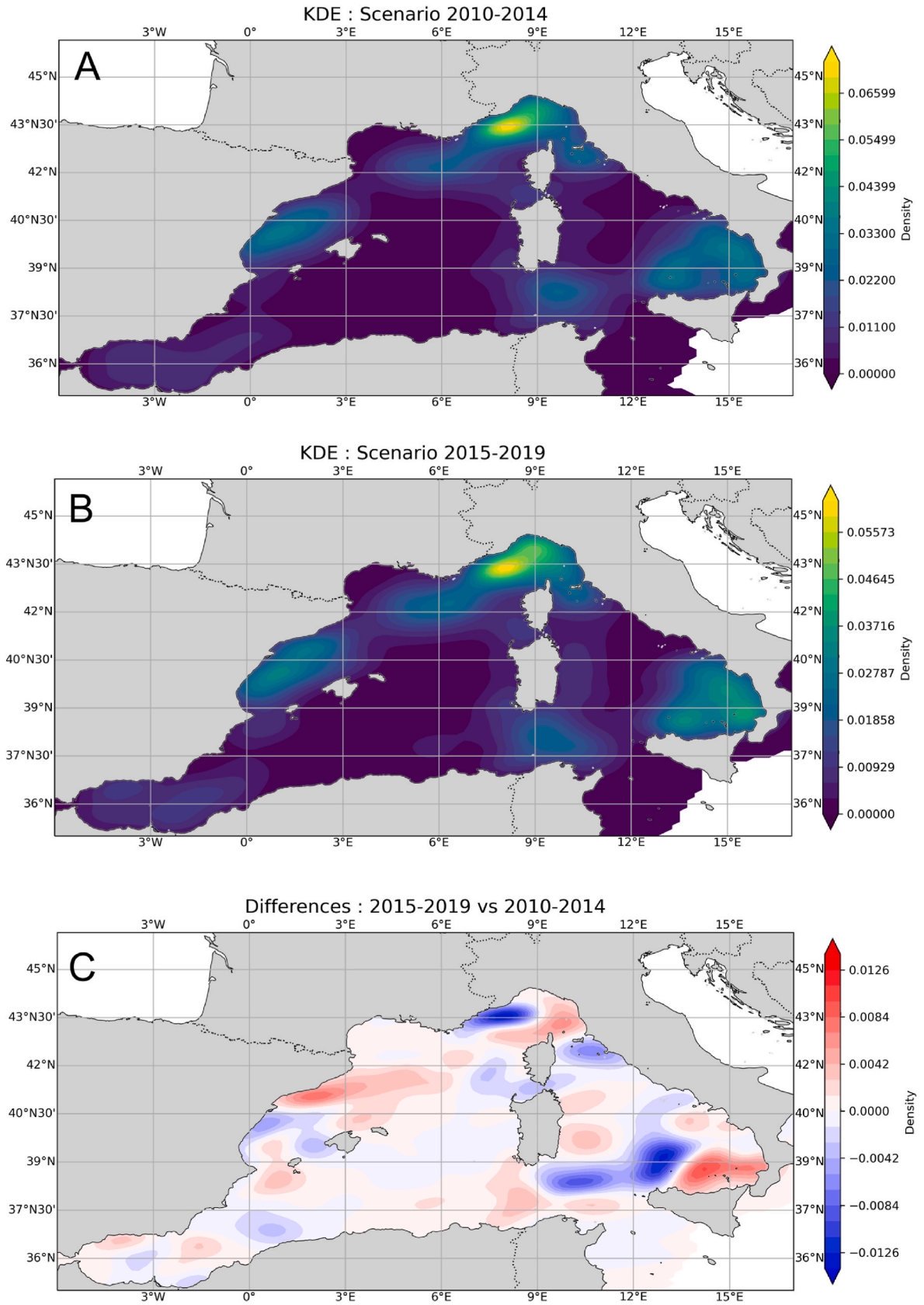

Fig. 7. Kernel density estimates (KDEs) of particle locations at the end of the PLD obtained using the MedMFC configuration for (A) 2010–2014 (B) 2015–2019 (C) shows the differences between the two time periods.

the KDE method. Regions of high density represent areas where larvae concentrate at the end of their PLD. The second map (Fig. 7B) corresponds to the 2015–2019 scenario and similarly visualizes the spatial distribution of larvae for this period. Lastly, the third difference map (Fig. 7C) (2015–2019 vs. 2010–2014) spatially highlights variations. Specifically, red zones indicate an increase in density during 2015–2019 compared to 2010–2014, while blue zones show a decrease in density during the same comparison.

The KDE map for 2010–2014 (Fig. 7A) shows higher maximum density values compared to the 2015–2019 scenario (Fig. 7B). However, the areas with the highest concentrations remain largely consistent between the two periods, particularly in the Ligurian Sea, the southern Tyrrhenian Sea, the Balearic Sea, and, to a lesser extent, the area between Tunisia and southern Sardinia. The difference map (Fig. 7C) highlights areas where larval densities increased during 2015–2019, such as the Spanish coasts near the France–Spain border (e.g., around zones SP8 and SP9), the northern Corsican coastline, and the coasts of the Ligurian Sea (e.g., NWCO, CAPi, IT1, FRI), as well as areas north of Sicily (e.g., SIC 1, 2, 3, USTi, EOLI, IT10, and IT9). Conversely, there are sectors where particle densities decreased over time, transitioning from the 2010–2014 to the 2015–2019 scenario, such as the Ligurian Sea's French coasts (e.g., FR1, FR2, FR3), the Bonifacio Strait south of Corsica (including Corsican and Sardinian zones SCO and NSA), and the southern Tyrrhenian Sea.

3.2.2. *Dispersal distances and orientations in a changing Mediterranean Sea*

The following analyses and results present two contrasting areas

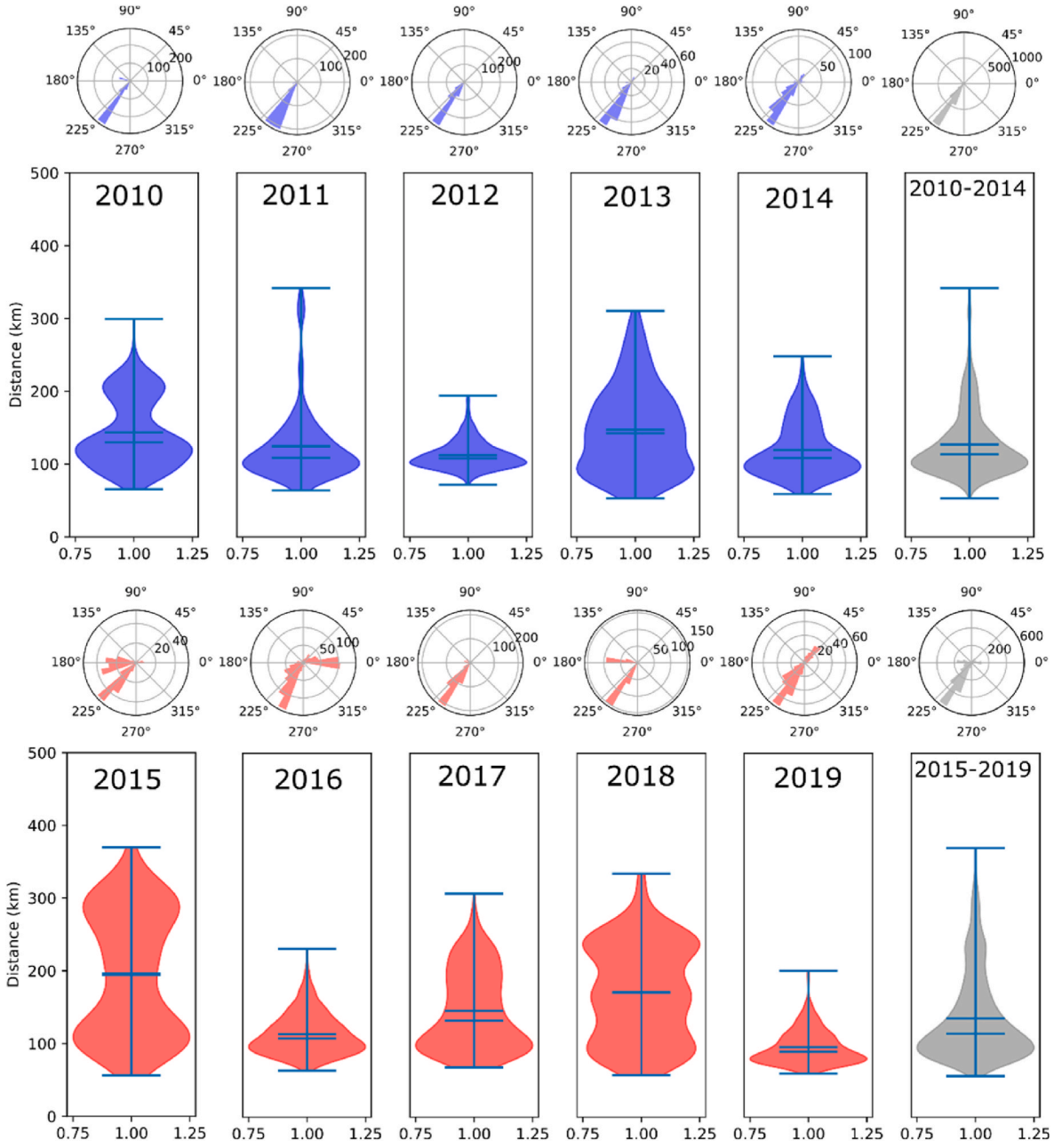

Fig. 8. Violin plots illustrating the distribution of distances traveled by larvae that successfully reached a recruitment area from the Catalan coast release zone (SP9; Fig. 2) across different time periods (2010–2014 in blue, with the average in grey, and 2015 to 2019, also with the average in grey). Wind roses depict the distribution of directions traveled by these larvae. Orientation is represented in cardinal directions: north (90°), south (270°), east (0°), and west (180°). (For interpretation of the references to color in this figure legend, the reader is referred to the Web version of this article.)

from the perspective of simulated connectivity and the status of *Maja squinado* in the Mediterranean. The Catalan coast or the France-Spain border (SP9; Fig. 2) is the area that connects the largest number of recruitment areas in the Balearic Islands, but with low connectivity percentages and high Gini indices (Fig. 6). Furthermore, the literature and supplementary approaches have demonstrated that *M. squinado* has almost disappeared from the Balearic Islands, rendering this area a primary focus of interest. This area contrasts with the Corsica-Sardinia zones were the spinous spider crab is still exploited. Consequently, it was decided to compare it in this analysis with the southwestern Corsica zone (SWCO; Fig. 2). The latter exhibits in the matrix a number of significant connections with other zones (Fig. 6). It is also included in what appears to be a cluster of larval exchange between Tunisia, Sardinia, Corsica, and the Ligurian Sea, in connection with other areas such as those in southern Corsica (SCO and SECO in Fig. 2).

The mean distance traveled by larvae from SP9 showed a slight increase, rising from 127.06 km (2010–2014) to 135.60 km (2015–2019). Additionally, the standard deviation of the distance increased from 44.35 km to 58.82 km, reflecting greater variability in the distances traveled. The standard deviation of the direction of travel also rose, from 57.59° to 83.01°, indicating increased variability in dispersal directions, although the mean resultant direction remained southeast for both time periods. Notably, the distribution of directions was bimodal in 2015, 2016, 2018, and 2019, in contrast to being unimodal during all years from 2010 to 2014 (Fig. 8). However, statistical analysis using the Kruskal-Wallis test revealed no significant differences in the distances traveled between the two periods (Appendix Table A2). This result suggests that, while variability in larval dispersal increased over time, the overall mean distances remained statistically consistent between the two scenarios.

The mean distance traveled by larvae was found to be slightly shorter during the 2015–2019 period (174.07 km) compared to the 2010–2014

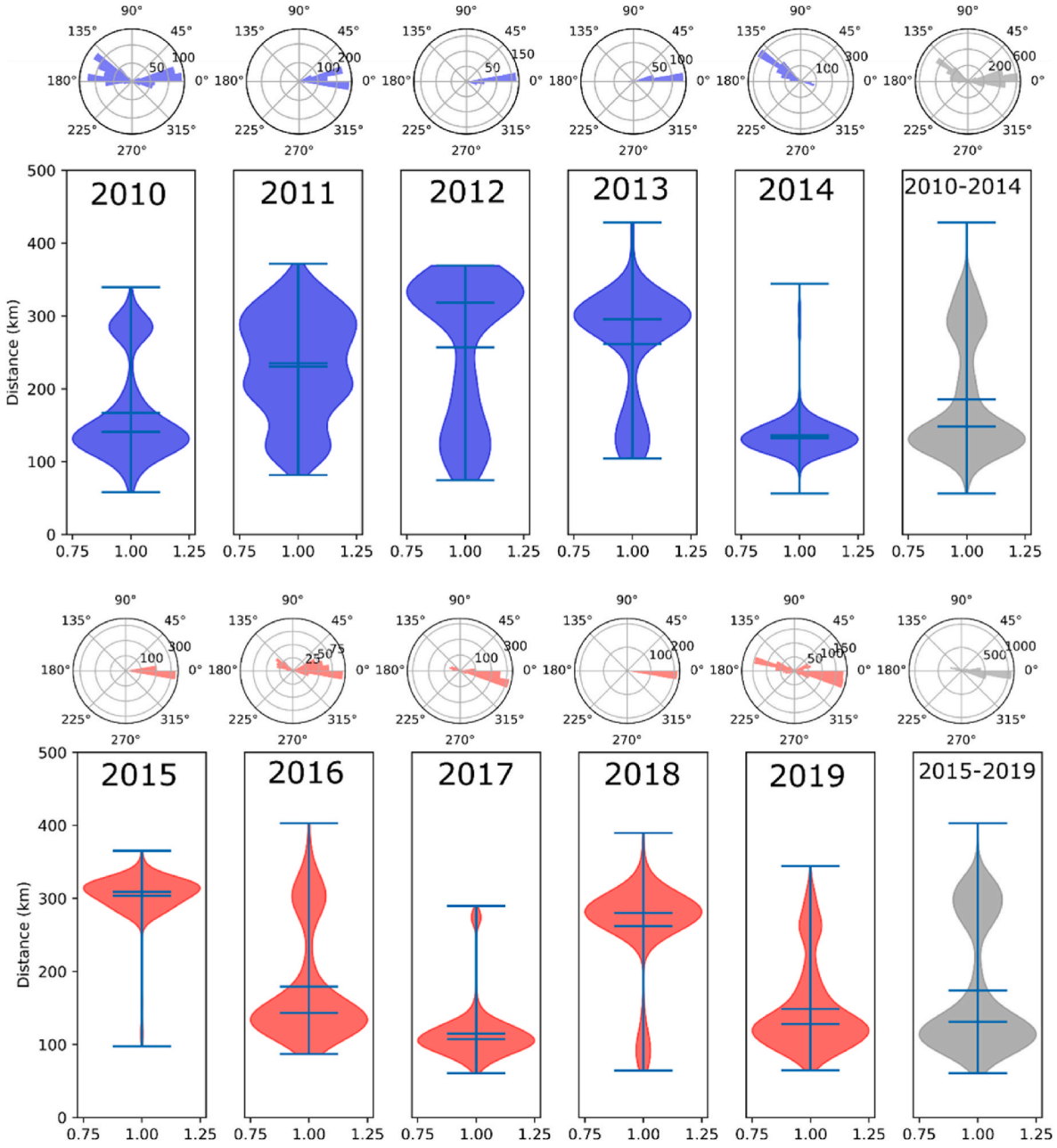

Fig. 9. Violin plots showing the distribution of distances traveled by larvae that have successfully reached a recruitment area from the Southwestern Corsican zone (SWCO; Fig. 2) for different time periods. Wind roses show the distribution of directions traveled by these larvae.

period (185.60 km), based on data from SWCO. However, the variability in distances traveled was greater during the 2015–2019 period, with a standard deviation of 85.23 km compared to 77.93 km in the 2010–2014 period. The mean direction of movement also exhibited a notable shift, from 58.51° to 1.10°, with increased directional variability during the 2015–2019 period. The mean dispersal direction averaged over the 2010–2014 period displayed two peaks: one at approximately 135° in the northwest direction and another at 0° in the eastward direction. In contrast, during the 2015–2019 period, only the 0° eastward direction peak was observed (Fig. 9).

Statistical analysis (detailed in Appendix Table A2) confirmed that the differences in distances traveled between the two periods were significant, as indicated by the Kruskal-Wallis test. Post hoc Dunn tests further revealed that significant differences in distances were consistently observed in multiple year-to-year comparisons. Notably, distances in later years (2015–2019) consistently differed from those in earlier years (2010–2014). For instance, 2015 showed significant differences compared to 2010, and 2019 differed significantly from 2010 as well. Importantly, the significant differences observed in the Dunn tests primarily involved comparisons between years that were far apart (e.g., 2010 vs. 2015 or 2017 vs. 2010), whereas adjacent years (e.g., 2013 vs. 2014) often showed no significant differences. This trend aligns with the statistical results presented in Appendix Table A2. Comparisons across intermediate years also showed significant differences, such as between 2013 and 2015 and between 2017 and 2015.

4. Discussion

This study aimed to improve our understanding of the dispersal dynamics and connectivity of *Maja squinado* in the Western Mediterranean, a species with contrasting population abundances due to overexploitation in some areas, while continuing to be fished along other coastlines. This work was conducted in the context of significant environmental changes in the Mediterranean, particularly the warming of surface waters. To achieve this, simulations were carried out using two hydrodynamic models, MedMFC and MARS3DMed, which provided complementary insights at different spatial resolutions.

The simulations generated by the MARS3DMed model are intended to reinforce and refine the findings observed in the MedMFC model simulations. This was made possible by meticulously delineating specific coastal exchanges, which could only be discerned with a higher level of detail. Consequently, the simulations are more closely aligned with field reality in the MARS3DMed model than in MedMFC, despite the broader geographic scope being essential to encompass pertinent release and recruitment sites. Indeed, research such as Swearer et al. (2019), emphasizes that current hydrodynamic models often lack the resolution needed to capture fine-scale dynamics in coastal zones, which can compromise the accuracy of larval dispersal predictions. Improving spatial resolution would allow models to better represent the physical processes that are most relevant at these scales. The literature converges on the finding, as highlighted by Putman and He (2013), that high-resolution models more closely align with field-observed trajectories, thereby enhancing the validity of predictions. Along this line, a recent study on Mediterranean gorgonian species larval dispersal simulations (Sciascia et al., 2022) in the Ligurian Sea identifies spatial resolution as the most influential factor in connectivity predictions, capturing both local-scale (larval processes) and regional-scale (population connectivity) dynamics. The authors underscore that finer resolutions yield better matches with empirical observations.

The results of simulations conducted in the Western Mediterranean have demonstrated, for the first time with a biophysical modelling approach at this spatiotemporal scale, that *Maja squinado*, with its relatively short PLD, exhibits limited dispersal capabilities. In general, the dispersion paths taken by the organism exhibit minimal variation over time, both in terms of distance and direction. These paths align with the predominant current patterns of the region and can be dispersed to distances exceeding eight times the average observed distance. Medium-scale oceanographic features, such as fronts and eddies, have been identified as key mechanisms affecting dispersion in these specific areas (Alcaraz et al., 2007). Although vertical migration is commonly accepted in crustaceans of the Brachyurans group, its effects were not tested in this study and were parameterised as active in our simulations. However, in other species, this migration has been demonstrated in the literature to constrain the distance and speed of dispersion (Zakardjian et al., 1999). As with other Brachyurans, larval dispersion and migration may be defined here by the dominant current patterns of the location (Anger et al., 2015), as well as the presence or absence of suitable habitats for spawning and recruitment.

In the presented study, observations were made in the context of the warming of surface waters in the Mediterranean, with particular attention paid to the acceleration observed between 2014 and 2015 (Margirier et al., 2020; Pastor et al., 2020). This warming is part of broader global and regional climatic trends that are increasingly recognized as key drivers of changes in oceanographic processes. Recent studies (Ser-Giacomi et al., 2020; de la Vara et al., 2022; Parras-Berrocal et al., 2024) further highlight that global and regional warming levels directly influence surface currents and their variability. These changes manifest through the intensification of turbulent activities, such as eddies, which are shaped by shifts in temperature as well as modifications in the direction and intensity of gyres.

Such physical changes in the ocean system are likely to have cascading effects on the connectivity and dispersal dynamics of marine species, particularly those with planktonic larval stages like *Maja squinado*. The graphical observations from this study illustrate these dynamics by showing differences between the two warming scenarios in the Mediterranean for the two subsampled areas, SP9 (France–Spain border zone) and SWCO (southwest Corsican coastal zone). The results suggest that warming-related changes in abiotic conditions could lead to shifts in the dispersal behaviours of *Maja squinado* larvae, with traditionally favorable areas for larval retention potentially becoming less suitable, while other regions may experience increased larval concentrations. To better understand these synergistic influences of global change on dispersal dynamics, future research should prioritize the collection of more extensive data, particularly in underrepresented areas like the Balearic Islands and their surrounding coastlines. These findings underscore the importance of continued investigations into the links between warming, hydrodynamic variability, and larval connectivity, as highlighted by the KDE results, which reinforce the hypothesis that accelerating sea surface temperature increases are reshaping dispersal trajectories and connectivity networks in the Mediterranean.

In addition to these physical drivers, another crucial link between global change and larval dispersion dynamics in *Maja squinado* lies in its biological responses to temperature. Temperature is likely a significant factor in conditioning spawning schedules, thereby affecting both the quality and quantity of eggs produced. For instance, studies have shown that ovarian mutations can be triggered by temperature changes in the freshwater shrimp *Penaeus merguiensis* (Hoang et al., 2002), while a study on brachyuran crabs found that rising temperatures tend to advance spawning periods (Azra et al., 2019). Similarly, temperature fluctuations have been shown to correlate with the spatial and temporal variation in the breeding cycles of the crab *Portunus armatus* (Johnson and Yeoh, 2021). However, no studies to date have specifically focused on *Maja squinado* in the Western Mediterranean to investigate its thermal tolerances and spawning schedule in the context of global change and warming sea surface temperatures. Future research into these biological responses would not only refine the calibration of dispersal models but also enhance our understanding of population dynamics in a rapidly changing Mediterranean ecosystem.

These findings highlight the complex interplay of environmental and biological factors, underscoring the need to view larval dispersal dynamics through the lens of a synergy rather than as a simple cause-and-effect relationship between global change and dispersal or connectivity

patterns. While current patterns remain the primary driver of larval dispersion for species with non-swimming larvae like *Maja squinado*, global warming-induced shifts in current regimes have cascading effects on zooplankton species and their dispersion. Numerous factors—including seasonal variations in currents, water temperature, and food availability—have been identified as critical to the survival and dispersal of crustacean larvae (Anger, 1991; Bryars and Havenhand, 2006; Epifanio & Garvine, 2001a). This study's findings suggest that even in the absence of warming scenarios, interannual variability in connectivity between sites is a key factor, likely exacerbated by global warming's effects on surface temperatures and current dynamics. A recommendation from the present study would be to incorporate these environmental and biological parameters into biophysical modeling in greater detail to enhance our understanding of observed dispersion patterns and to better elucidate the role of global change in driving interannual variability (Corrochano-Fraile et al., 2022; Šargač et al., 2022).

These predictions, when considered alongside the population dynamics of an exploited species with an IUCN status of non-evaluated, offer valuable insights that could contribute to the development of future management measures. Nonetheless, the predictions of the current model remain preliminary. While the model provides critical information about broad dispersal pathways, their temporal variability, and the connectivity relationships between essential habitats for *Maja squinado*, as well as hypotheses regarding the synergy between biotic and abiotic factors associated with global change, it requires further refinement to generate robust results suitable for management applications. Indeed, as models are adapted to nearshore environments, downscaling will be essential to better capture small-scale physical processes. However, this necessitates extensive field validation and calibration to ensure their accuracy and reliability (Taebi et al., 2012). The need for enhanced parameterization of both physical and biological components is emphasized as a crucial step for producing predictions that can effectively inform management strategies (Swearer et al., 2019). It is also highlighted that coarse-resolution models may fail to accurately represent coastal currents and local dynamics. This limitation represents a significant source of uncertainty in predictions used to guide the design of marine protected areas (Sciascia et al., 2022). Furthermore, the sensitivity of dispersal estimates to the spatial and temporal resolution of ocean circulation models remains a critical issue. Putman and He (2013) demonstrated that averaging model outputs over coarser resolutions can obscure key oceanographic processes, potentially leading to dispersal trajectories that could diverge from observed drifter paths.

The findings of this study enable the prediction of large-scale and long-term trends in *Maja squinado*, a species whose ecology and population dynamics remain poorly understood. Along the coasts where areas favorable to the spawning of the spinous spider crab have been parameterized, connectivity over multiple sites can occur between relatively distant locations through various intermediaries. It is likely that these coastal zones exhibit small-scale circulation dynamics that trap larvae near the release site, influenced by interactions with eddies and seafloor topography. Sites with high local retention can maintain significant local recruitment, supporting a population over time and reducing the risk of larval loss or recruitment failure due to phenotype-environment mismatches (King et al., 2023). Based on the selected release sites, larval exchanges in the Mediterranean appear to be confined within distinct basins. For instance, there is a scarcity of larval exchanges between the Algero-Provençal basin and the Tyrrhenian Sea via the Ligurian Sea. Similarly, the Alboran Sea and the Balearic Islands appear isolated from the rest of the coastlines. With the exception of the Northwestern Mediterranean, where connectivity between Corsica, Italy, and the French coastlines is consistent and regular over the study period, it is challenging to estimate links between more distant sites due to the relatively short larval duration of the spider crab. There is almost no observable connection between Catalonia and the Balearic Islands, suggesting low connectivity with these islands. This isolation can be attributed to the hydrodynamically complex nature of the Balearic Sea, resulting from interactions between different water masses and the island's topography, which limits species exchange between these areas and other regions (López-Jurado et al., 1995; Pinot et al., 2002). This research contributes to our understanding of the exploitation and preservation challenges of *M. squinado* in the Mediterranean by offering initial observations on connectivity and population dynamics, highlighting the constraints on larval exchanges within the Mediterranean's distinct basins.

The reliability and significance of predictions derived from biophysical models are increasingly apparent when compared to alternative scientific methodologies. Consequently, population genetic studies on *Maja squinado* could offer invaluable insights to refine and enhance the parameterization of future simulations. For instance, such studies could improve our understanding of the species' dispersal patterns by identifying specific sub-populations around islands and across broader spatial scales. However, this integration is not straightforward. As studies have demonstrated, the genetic structures observed in populations often reflect cumulative gene flow over multiple generations, a dynamic that single-generation dispersal models are unable to capture (Jahnke et al., 2018). Multi-generational dispersal models, by incorporating cumulative implicit links (e.g., siblings sharing a common ancestor) and stepping-stone dynamics, offer a more robust approach to understanding connectivity across larger spatial and temporal scales (Ser-Giacomi et al., 2021). Moreover, such models have the potential to challenge traditional assumptions of strict isolation imposed by physical barriers such as gyres or strong currents, instead revealing indirect connectivity through intermediate stepping-stones (Pascual et al., 2017).

Nevertheless, these genetic insights complement, rather than replace, biophysical approaches. For example, while this study focuses on larval dispersal, it is critical to acknowledge the multitude of factors influencing larval recruitment, including predation, competition, and ontogenetic traits (Anger et al., 2015). Larvae may serve as a resource for some species while simultaneously being preyed upon by others, further complicating recruitment success (Anger et al., 2015; Torres et al., 2013). The present model does not incorporate factors affecting larval mortality, which are often driven by interspecific relationships. Future simulations would benefit from additional studies aimed at refining these parameters. For instance, it would be particularly valuable to quantify the quality and quantity of spawning events and to identify the biotic and abiotic factors influencing the survival of larval cohorts across different years. Such advancements would significantly improve the predictive power and ecological relevance of biophysical models, making them better suited for applications in conservation and fisheries management.

The findings of this study highlight that the ability to identify source and sink sites within the dispersal system is critical. From a management perspective, understanding the dispersal characteristics of these sites is essential for assessing their significance within a localized system. For instance, sites that release more larvae than they retain may be particularly vulnerable to population collapse due to overfishing, as this can reduce the number of larvae available to replenish other areas (Cowen et al., 2002; Steneck, 2006). This issue is especially relevant for the Balearic Islands, which experience limited larval recruitment from Spain and potentially the Maghreb, while also facing significant fishing pressure (Garcia, 2007). The predominance of short-distance larval dispersal, compared to other species with higher dispersal ranges that raise concerns for invasions, prompts questions about the role of islands in broader species dispersal dynamics.

Areas characterized by high connectivity, such as the Corsican and Sardinian coastlines, along with Sicily, Tunisia, and southern Sardinia, offer promising opportunities for studies on the benefits of establishing a network of marine protected areas (MPAs). Such a network would safeguard larval exchange and sustain pools of breeding individuals, thereby reducing the risk of population collapses in regions that are

overly isolated and cut off from larval exchanges. For example, the depleted stocks and subsequent cessation of fishing activities observed in the Balearic Islands serve as a cautionary example of what can happen in the absence of robust larval connectivity.

These findings could be further corroborated by genetic and phylogenetic studies, which would provide insights into genetic differentiation and relatedness between populations, ultimately revealing the existence of distinct sub-populations. Such genetic studies have already been conducted on the sister species *Maja brachydactyla* in the Atlantic, where the importance of the Strait of Gibraltar in defining species boundaries has been demonstrated (Abelló et al., 2014). Identifying genetic barriers and patterns of gene flow would offer valuable indicators for assessing larval dispersal and differentiation between populations (Gilg and Hilbish, 2003). This information is vital for the design of effective MPAs and the identification of nursery zones crucial to the conservation and management of *Maja squinado*.

5. Conclusion

This study represents the first larval dispersal model of *Maja squinado* on a Western Mediterranean scale. Our analyses, combining graphical observations, have provided insights into the dispersal patterns and potential impacts of climate change on the larval stages of this commercially exploited species. The relatively short pelagic larval duration (PLD) of *Maja squinado* likely explains the observed relationship between the disappearance of the species in heavily fished areas and poorly connected zones. For example, the Balearic Islands, which are geographically isolated, do not consistently connect with other coastal areas due to the limited pelagic larval duration of the spinous spider crab. This isolation could be a primary factor in the species' decline in these regions. However, this hypothesis requires further investigation, including genetic analyses, to better understand the level of population isolation. The predictions from our simulations allow us to observe interannual changes, especially in the context of post-warming acceleration shifts. It is of the utmost importance to incorporate these climatic considerations into future models, as global changes not only affect the dynamics of ocean currents, which are crucial for larval dispersal, but also directly impact the physiology of the modeled organisms. Our results emphasize the necessity to integrate biophysical modelling approaches with other methodologies, particularly genetic studies. For instance, it is of the utmost importance to determine whether the populations within the Sardinia-Corsica cluster are homogeneous or exhibit significant genetic differentiation. Such combined approaches will provide a more comprehensive understanding of the population dynamics and connectivity of *Maja squinado*. In conclusion, while the current study provides valuable insights, it also highlights the necessity for multidisciplinary research to address the complex interactions between environmental changes, species physiology, and population connectivity.

CRediT authorship contribution statement

C. Barrier: Writing – review & editing, Writing – original draft, Visualization, Validation, Methodology, Investigation, Formal analysis, Data curation, Conceptualization, Writing – review & editing, Writing – original draft, Visualization, Methodology, Investigation, Formal analysis, Data curation, Conceptualization. **T. Beneteau:** Writing – review & editing, Methodology, Investigation, Data curation, Conceptualization. **M.-C. Raffalli:** Writing – review & editing. **N. Barrier:** Writing – review & editing, Software, Methodology. **C. Lett:** Writing – review & editing, Software, Methodology. **V. Pasqualini:** Writing – review & editing, Supervision, Methodology. **E.D.H. Durieux:** Writing – review & editing, Supervision, Methodology.

Declaration of competing interest

The authors declare that they have no known competing financial interests or personal relationships that could have appeared to influence the work reported in this paper.

Appendices.

A1: The sea surface temperature data extracted from the Copernicus Marine Environment Monitoring Service (CMEMS) satellite product over the western Mediterranean Sea demonstrated a temperature increase trend of 0.034 ± 0.002 °C per year, with a 95% confidence interval. To analyze trends spatially and focus on the last decade, data from the Med MFC physical multiyear product (Mediterranean Sea Physics Reanalysis) were examined at all points in the Western Mediterranean (focusing on our study window). A linear temperature trend was calculated for each grid point based on time series data through linear regression. A color gradient from blue (indicating a decrease in temperature) to red (indicating an increase in temperature) was used to map these trends. The detailed analysis is presented in figure A1 below.

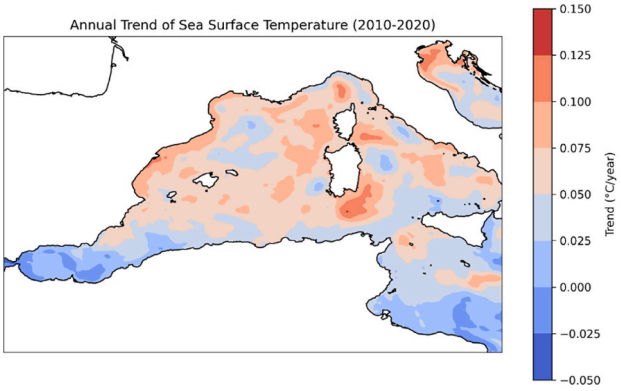

Fig. A1. Sea Surface Temperature Trends in the Western Mediterranean from 2010 to 2020. This map illustrates the decadal trend in sea surface temperatures, with the color scale ranging from −0.050 °C (blue) to +0.150 °C (red), highlighting areas of temperature decrease and increase relative to the period average.

A2: Table of statistical test results for larval dispersal distances: this table presents the results of three statistical analyses applied to the distances traveled by larvae successfully reaching potential recruitment areas, originating from selected zones: SP9 (France-Spain border) and SWCO (south-western coast of Corsica). The tests include the Shapiro-Wilk test for normality, the Kruskal-Wallis test for differences between distributions, and Dunn's post hoc test (with Bonferroni correction applied). The significance threshold was set at $\alpha = 0.05$. Results detail whether the normality

assumption was met, significant differences were found between scenarios, and pairwise comparisons yielded statistically significant results.

Zone	Period	Test	P-value	Result
SP9	2010–2014	Shapiro-Wilk	<1e-42	Non normal
SP9	2015–2019	Shapiro-Wilk	<1e-43	Non normal
SP9	2010–2014 vs 2015–2019	Kruskal-Wallis	0.374	Non significant
SWCO	2010–2014	Shapiro-Wilk	<1e-49	Non normal
SWCO	2015–2019	Shapiro-Wilk	<1e-51	Non normal
SWCO	2010–2014 vs 2015–2019	Kruskal-Wallis	<1e-42	Significant
SWCO	2010 vs 2010	Dunn	1.0	Non significant
SWCO	2011 vs 2010	Dunn	<1e-47	Significant
SWCO	2012 vs 2010	Dunn	<1e-39	Significant
SWCO	2013 vs 2010	Dunn	<1e-37	Significant
SWCO	2014 vs 2010	Dunn	0.0	Significant
SWCO	2015 vs 2010	Dunn	<1e-143	Significant
SWCO	2016 vs 2010	Dunn	0.052	Non significant
SWCO	2017 vs 2010	Dunn	<1e-114	Significant
SWCO	2018 vs 2010	Dunn	<1e-28	Significant
SWCO	2019 vs 2010	Dunn	<1e-12	Significant
SWCO	2010 vs 2011	Dunn	<1e-47	Significant
SWCO	2011 vs 2011	Dunn	1.0	Non significant
SWCO	2012 vs 2011	Dunn	0.275	Non significant
SWCO	2013 vs 2011	Dunn	0.031	Significant
SWCO	2014 vs 2011	Dunn	<1e-100	Significant
SWCO	2015 vs 2011	Dunn	<1e-32	Significant
SWCO	2016 vs 2011	Dunn	<1e-16	Significant
SWCO	2017 vs 2011	Dunn	<1e-287	Significant
SWCO	2018 vs 2011	Dunn	1.0	Non significant
SWCO	2019 vs 2011	Dunn	<1e-106	Significant
SWCO	2010 vs 2012	Dunn	<1e-39	Significant
SWCO	2011 vs 2012	Dunn	0.275	Non significant
SWCO	2012 vs 2012	Dunn	1.0	Non significant
SWCO	2013 vs 2012	Dunn	1.0	Non significant
SWCO	2014 vs 2012	Dunn	<1e-72	Significant
SWCO	2015 vs 2012	Dunn	<1e-10	Significant
SWCO	2016 vs 2012	Dunn	<1e-19	Significant
SWCO	2017 vs 2012	Dunn	<1e-185	Significant
SWCO	2018 vs 2012	Dunn	1.0	Non significant
SWCO	2019 vs 2012	Dunn	<1e-77	Significant
SWCO	2010 vs 2013	Dunn	<1e-37	Significant
SWCO	2011 vs 2013	Dunn	0.031	Significant
SWCO	2012 vs 2013	Dunn	1.0	Non significant
SWCO	2013 vs 2013	Dunn	1.0	Non significant
SWCO	2014 vs 2013	Dunn	<1e-65	Significant
SWCO	2015 vs 2013	Dunn	0.0	Significant
SWCO	2016 vs 2013	Dunn	<1e-19	Significant
SWCO	2017 vs 2013	Dunn	<1e-162	Significant
SWCO	2018 vs 2013	Dunn	1.0	Non significant
SWCO	2019 vs 2013	Dunn	<1e-70	Significant
SWCO	2010 vs 2014	Dunn	0.0	Significant
SWCO	2011 vs 2014	Dunn	<1e-100	Significant
SWCO	2012 vs 2014	Dunn	<1e-72	Significant
SWCO	2013 vs 2014	Dunn	<1e-65	Significant
SWCO	2014 vs 2014	Dunn	1.0	Non significant
SWCO	2015 vs 2014	Dunn	<1e-218	Significant
SWCO	2016 vs 2014	Dunn	<1e-15	Significant
SWCO	2017 vs 2014	Dunn	<1e-61	Significant
SWCO	2018 vs 2014	Dunn	<1e-52	Significant
SWCO	2019 vs 2014	Dunn	1.0	Non significant
SWCO	2010 vs 2015	Dunn	<1e-143	Significant
SWCO	2011 vs 2015	Dunn	<1e-32	Significant
SWCO	2012 vs 2015	Dunn	<1e-10	Significant
SWCO	2013 vs 2015	Dunn	0.0	Significant
SWCO	2014 vs 2015	Dunn	<1e-218	Significant
SWCO	2015 vs 2015	Dunn	1.0	Non significant
SWCO	2016 vs 2015	Dunn	<1e-78	Significant
SWCO	2017 vs 2015	Dunn	<1e-300	Significant
SWCO	2018 vs 2015	Dunn	0.0	Significant
SWCO	2019 vs 2015	Dunn	<1e-224	Significant
SWCO	2010 vs 2016	Dunn	0.052	Non significant
SWCO	2011 vs 2016	Dunn	<1e-16	Significant
SWCO	2012 vs 2016	Dunn	<1e-19	Significant
SWCO	2013 vs 2016	Dunn	<1e-19	Significant
SWCO	2014 vs 2016	Dunn	<1e-15	Significant
SWCO	2015 vs 2016	Dunn	<1e-78	Significant
SWCO	2016 vs 2016	Dunn	1.0	Non significant

(*continued on next page*)

(*continued*)

Zone	Period	Test	P-value	Result
SWCO	2017 vs 2016	Dunn	<1e-99	Significant
SWCO	2018 vs 2016	Dunn	<1e-13	Significant
SWCO	2019 vs 2016	Dunn	<1e-18	Significant
SWCO	2010 vs 2017	Dunn	<1e-114	Significant
SWCO	2011 vs 2017	Dunn	<1e-287	Significant
SWCO	2012 vs 2017	Dunn	<1e-185	Significant
SWCO	2013 vs 2017	Dunn	<1e-162	Significant
SWCO	2014 vs 2017	Dunn	<1e-61	Significant
SWCO	2015 vs 2017	Dunn	<1e-300	Significant
SWCO	2016 vs 2017	Dunn	<1e-99	Significant
SWCO	2017 vs 2017	Dunn	1.0	Non significant
SWCO	2018 vs 2017	Dunn	<1e-139	Significant
SWCO	2019 vs 2017	Dunn	<1e-50	Significant
SWCO	2010 vs 2018	Dunn	<1e-28	Significant
SWCO	2011 vs 2018	Dunn	1.0	Non significant
SWCO	2012 vs 2018	Dunn	1.0	Non significant
SWCO	2013 vs 2018	Dunn	1.0	Non significant
SWCO	2014 vs 2018	Dunn	<1e-52	Significant
SWCO	2015 vs 2018	Dunn	0.0	Significant
SWCO	2016 vs 2018	Dunn	<1e-13	Significant
SWCO	2017 vs 2018	Dunn	<1e-139	Significant
SWCO	2018 vs 2018	Dunn	1.0	Non significant
SWCO	2019 vs 2018	Dunn	<1e-56	Significant
SWCO	2010 vs 2019	Dunn	<1e-12	Significant
SWCO	2011 vs 2019	Dunn	<1e-106	Significant
SWCO	2012 vs 2019	Dunn	<1e-77	Significant
SWCO	2013 vs 2019	Dunn	<1e-70	Significant
SWCO	2014 vs 2019	Dunn	1.0	Non significant
SWCO	2015 vs 2019	Dunn	<1e-224	Significant
SWCO	2016 vs 2019	Dunn	<1e-18	Significant
SWCO	2017 vs 2019	Dunn	<1e-50	Significant
SWCO	2018 vs 2019	Dunn	<1e-56	Significant
SWCO	2019 vs 2019	Dunn	1.0	Non significant

Data availability

Data will be made available on request.

References

Abelló, P., Guerao, G., Salmerón, F., Raso, J.E.G., 2014. *Maja brachydactyla* (Brachyura: Majidae) in the western mediterranean. Marine Biodiversity Records 7, e77.

Adams, D.K., Arellano, S.M., Govenar, B., 2012. Larval dispersal: vent life in the water column. Oceanography (Wash., D.C.) 25 (1), 256–268.

Alcaraz, M., Calbet, A., Estrada, M., Marrasé, C., Saiz, E., Trepat, I., 2007. Physical control of zooplankton communities in the Catalan Sea. Prog. Oceanogr. 74 (2–3), 294–312.

Al-Qattan, N., Herbert, G.S., Spero, H.J., McCarthy, S., McGeady, R., Tao, R., Power, A. M., 2023. A stable isotope sclerochronology-based forensic method for reconstructing debris drift paths with application to the MH370 crash. AGU Advances 4 (4), e2023AV000915.

Angeletti, R., Binato, G., Guidotti, M., Morelli, S., Pastorelli, A.A., Sagratella, E., et al., 2014. Cadmium bioaccumulation in Mediterranean spider crab (*Maja squinado*): human consumption and health implications for exposure in Italian population. Chemosphere 100, 83–88.

Anger, K., 1991. Effects of temperature and salinity on the larval development of the Chinese mitten crab *Eriocheir sinensis* (Decapoda: Grapsidae). Marine ecology progress series. Oldendorf 72 (1), 103–110.

Anger, K., Queiroga, H., Calado, R., 2015. Larval development and behaviour strategies in Brachyura. In: Treatise on Zoology-Anatomy, Taxonomy, Biology. The Crustacea, Volume 9 Part C (2 Vols). Brill, pp. 317–374.

Arakawa, A., Lamb, V.R., 1977. In: Chang, J. (Ed.), Methods in Computational Physics : Advances in Research and Applications, Vol. 17. Elsevier, pp. 173–265. https://doi.org/10.1016/B978-0-12-460817-7.50009-4.

Azra, M.N., Chen, J.C., Hsu, T.H., Ikhwanuddin, M., Abol-Munafi, A.B., 2019. Growth, molting duration and carapace hardness of blue swimming crab, *Portunus pelagicus*, instars at different water temperatures. Aquaculture reports 15, 100226.

Balss, H., 1922. Crustacea VII: Decapoda Brachyura (Oxyrhyncha und Brachyrhyncha) und geographische Übersicht über Crustacea Decapoda. In: Michaelsen, W. (Ed.), Beiträge zur Kenntnis der Meeresfauna Westafrikas. Friederichsen and Co, Hamburg, pp. 69–110.

Begon, M., ownsend, C., arper, J., 2005. Ecology: rom individuals to ecosystems. Freshwater Biology—FRESHWATER BIOL 51.

Bianchi, C.N., Morri, C., 2000. Marine biodiversity of the Mediterranean Sea: situation, problems and prospects for future research. Mar. Pollut. Bull. 40 (5), 367–376.

Bousquet, C., Bouet, M., Patrissi, M., Cesari, F., Lanfranchi, J.B., Susini, S., et al., 2022. Assessment of catch composition, production and fishing effort of small-scale fisheries: the case study of Corsica Island (Mediterranean Sea). Ocean Coast Manag. 218, 105998.

Bryars, S.R., Havenhand, J.N., 2006. Effects of constant and varying temperatures on the development of blue swimmer crab (*Portunus pelagicus*) larvae: laboratory observations and field predictions for temperate coastal waters. J. Exp. Mar. Biol. Ecol. 329 (2), 218–229.

Calado, R., Guerao, G., Gras, N., Cleary, D.F., Rotllant, G., 2013. Contrasting habitats occupied by sibling spider crabs *Maja squinado* and *Maja brachydactyla* (Brachyura, Majidae) can influence the biochemical variability displayed by newly hatched larvae. J. Plankton Res. 35 (3), 684–688.

Carlson, A., Maynou, F., Basurco, B., Bernal, M., 2016. Chapitre 2-Gestion des ressources marines vivantes. In: Mediterra 2016 : Zéro gaspillage en Méditerranée. Presses de Sciences Po, pp. 51–70. Coll et al., 2014.

Corrochano-Fraile, A., Adams, T.P., Aleynik, D., Bekaert, M., Carboni, S., 2022. Predictive biophysical models of bivalve larvae dispersal in Scotland. Front. Mar. Sci. 9, 985748.

Cowen, R.K., Gawarkiewicz, G., Pineda, J., Thorrold, S., Werner, F., 2002. Population connectivity in marine systems. Report of a workshop to develop science recommendations for the National Science Foundation 84, 119-119.

de la Vara, A., Parras-Berrocal, I.M., Izquierdo, A., Sein, D.V., Cabos, W., 2022. Climate change signal in the ocean circulation of the Tyrrhenian Sea. Earth System Dynamics 13 (1), 303–319.

de Mello, C., Barreiro, M., Hernandez-Garcia, E., Trinchin, R., Manta, G., 2023. A Lagrangian study of summer upwelling along the Uruguayan coast. Cont. Shelf Res. 258, 104987.

DeAngelis, D.L., Mooij, W.M., 2005. Individual-based modeling of ecological and evolutionary processes. Annual Review of Ecology, Evolution, and Systematics 36, 147–168.

Durán, J., Palmer, M., Pastor, E., 2013. Growing reared spider crabs (*Maja squinado*) to sexual maturity: the first empirical data and a predictive growth model. Aquaculture 408, 78–87.

Durán, J., Pastor, E., Grau, A., Valencia, J.M., 2012. First results of embryonic development, spawning and larval rearing of the Mediterranean spider crab *Maja squinado* (Herbst) under laboratory conditions, a candidate species for a restocking program. Aquac. Res. 43 (12), 1777–1786.

Epifanio, C.E., Garvine, R.W., 2001. Larval transport on the atlantic continental shelf of north America: a review. Estuar. Coast Shelf Sci. 52, 51–77. https://doi.org/10.1006/ecss.2000.0727.

Escudier, R., Clementi, E., Cipollone, A., Pistoia, J., Drudi, M., Grandi, A., Lyubartsev, V., Lecci, R., Aydogdu, A., Delrosso, D., Omar, M., Masina, S., Coppini, G., Pinardi, N.,

2021. A high resolution reanalysis for the Mediterranean Sea. Front. Earth Sci. 9. https://www.frontiersin.org/articles/10.3389/feart.2021.702285.
FAO, 2020. La situation mondiale des pêches et de l'aquaculture 2020 : La durabilité an action. FAO. https://doi.org/10.4060/ca9229fr.
Flores-Valiente, J., Lett, C., Colas, F., Pecquerie, L., Aguirre-Velarde, A., Rioual, F., et al., 2023. Influence of combined temperature and food availability on Peruvian anchovy (*Engraulis ringens*) early life stages in the northern Humboldt Current system: a modelling approach. Prog. Oceanogr. 215, 103034.
Garcia, L., 2007. Garcia Ll (2007) Els crancs de les Balears. In: Documenta Balear, S.L. (Ed.), Quaderns de Natura de les Balears. Palma de Mallorca, p. 104.
Gary, S.F., Fox, A.D., Biastoch, A., Roberts, J.M., Cunningham, S.A., 2020. Larval behaviour, dispersal and population connectivity in the deep sea. Sci. Rep. 10 (1). https://doi.org/10.1038/s41598-020-67503-7. Article 1.
Gatti, J., Pairaud, I., 2010. Optimisation échantillonnage in situ: Qualification des configurations méditerranéennes du modèle MARS3D.
Gilg, M.R., Hilbish, J., 2003. The Geography of marine larval dispersal: coupling genetics with fine-scale physical oceanography. Ecology 84 (11), 2989–2998. https://doi.org/10.1890/02-0498.
Gualtieri, J.-S., Aiello, A., Antoine-Santoni, T., Poggi, B., DeGentili, E., 2013. Active tracing of *Maja squinado* in the Mediterranean Sea with wireless acoustic sensors: method, results and prospectives. Sensors (Basel, Switzerland) 13 (11), 15682–15691. https://doi.org/10.3390/s131115682.
Guerao, G., Rotllant, G., 2010. Development and growth of the early juveniles of the spider crab *Maja squinado* (Brachyura: majoidea) in an individual culture system. Aquaculture 307 (1–2), 105–110.
Guerao, G., Rotllant, G., Gisbert, E., Uyà, M., Cardona, L., 2016. Consistent habitat segregation between sexes in the spider crabs *Maja brachydactyla* and *Maja squinado* (Brachyura), as revealed by stable isotopes. Sci. Mar. 80. https://doi.org/10.3989/scimar.04236.23B.
Herbst, J.F.W., 1788. Versuch einer Naturgeschichte der Krabben und Krebse nebst einer systematischen Beschreibung ihrer verschiede-nen Arten. Lange, G.A., Berlin and Stralsund, pp. 207–238.
Hixon, M.A., Jones, G.P., 2005. Competition, predation, and density-dependent mortality in demersal marine fishes. Ecology 86 (11), 2847–2859. https://doi.org/10.1890/04-1455.
Hoang, T., Lee, S.Y., Keenan, C.P., Marsden, G.E., 2002. Effect of temperature on spawning of Penaeus merguiensis. J. Therm. Biol. 27 (5), 433–437.
Imzilen, T., Kaplan, D.M., Barrier, N., Lett, C., 2023. Simulations of drifting fish aggregating device (dFAD) trajectories in the Atlantic and Indian Oceans. Fish. Res. 264, 106711. https://doi.org/10.1016/j.fishres.2023.106711.
Jahnke, M., Jonsson, P.R., 2022. Biophysical models of dispersal contribute to seascape genetic analyses. Phil. Trans. Biol. Sci. 377 (1846), 20210024. https://doi.org/10.1098/rstb.2021.0024.
Jahnke, M., Jonsson, P.R., Moksnes, P.O., Loo, L.O., Nilsson Jacobi, M., Olsen, J.L., 2018. Seascape genetics and biophysical connectivity modelling support conservation of the seagrass Zostera marina in the Skagerrak–Kattegat region of the eastern North Sea. Evolutionary applications 11 (5), 645–661.
Johnston, D.J., Yeoh, D.E., 2021. Temperature drives spatial and temporal variation in the reproductive biology of the blue swimmer crab *Portunus armatus* A. Milne-Edwards, 1861 (Decapoda: Brachyura: portunidae). J. Crustac Biol. 41 (3), ruab032.
King, S., Saint-Amand, A., Walker, B.K., Hanert, E., Figueiredo, J., 2023. Larval dispersal patterns and connectivity of Acropora on lorida's Coral Reef and its implications for restoration. Front. Mar. Sci. 9. https://www.frontiersin.org/articles/10.3389/fmars.2022.1038463.
Lazure, P., Dumas, F., 2008. An external–internal mode coupling for a 3D hydrodynamical model for applications at regional scale (MARS). Adv. Water Resour. 31 (2), 233–250. https://doi.org/10.1016/j.advwatres.2007.06.010.
Lett, C., Ayata, S.-D., Huret, M., Irisson, J.-O., 2010. Biophysical modelling to investigate the effects of climate change on marine population dispersal and connectivity. Prog. Oceanogr. 87, 106–113. https://doi.org/10.1016/j.pocean.2010.09.005.
Lett, C., Verley, P., Mullon, C., Parada, C., Brochier, T., Penven, P., Blanke, B., 2008. A Lagrangian tool for modelling ichthyoplankton dynamics. Environ. Model. Software 23 (9), 1210. https://doi.org/10.1016/j.envsoft.2008.02.005.
López-Jurado, J.L., García-Lafuente, J.M., Cano-Lucaya, N., 1995. Hydrographic conditions of the ibiza channel during november 1990, march 1991 and july 1992. https://digital.csic.es/handle/10261/317533.
Marengo, M., Pere, A., Marchand, B., Lejeune, P., Durieux, E., 2016. Catch variation and demographic structure of common dentex (Sparidae) exploited by Mediterranean artisanal fisheries. Bull. Mar. Sci. 92. https://doi.org/10.5343/bms.2015.1041.
Marengo, M., Vanalderweireldt, L., Horri, K., Patrissi, M., Santoni, M.-C., Lejeune, P., Durieux, E., 2023. Combining indicator trends to evaluate a typical Mediterranean small-scale fishery: a case study of Corsica. Regional Studies in Marine Science 65, 103087. https://doi.org/10.1016/j.rsma.2023.103087.
Margirier, F., Testor, P., Heslop, E., Mallil, K., Bosse, A., Houpert, L., et al., 2020. Abrupt warming and salinification of intermediate waters interplays with decline of deep convection in the Northwestern Mediterranean Sea. Sci. Rep. 10 (1), 20923.
Martín, P., Maynou, F., Stelzenmüller, V., Sacanell, M., 2012. A small-scale fishery near a rocky littoral marine reserve in the northwestern Mediterranean (Medes Islands) after two decades of fishing prohibition. Sci. Mar. 76. https://doi.org/10.3989/scimar.03471.07F.
Millot, C., Taupier-Letage, I., 2005. Circulation in the Mediterranean Sea. In: Saliot, A. (Ed.), The Mediterranean Sea. Springer, pp. 29–66. https://doi.org/10.1007/b107143.
Modena, M., Mori, M., Vacchi, M., 2001. Note su alcuni crostacei malacostraci raccolti in aree adiacenti alla M/C Haven (Mar Ligure). Biol. Mar. Mediterr. 8, 675–679.
Mura, M., Corda, S., 2011. Crustacea Decapoda in the Sardinian Channel: a checklist. Crustaceana 84 (5–6), 667–687.
Neumann, V., 1998. A review of the *Maja squinado* (Crustacea: Decapoda: Brachyura) species-complex with a key to the eastern Atlantic and Mediterranean species of the genus. J. Nat. Hist. 32 (10–11), 1667–1684. https://doi.org/10.1080/00222939800771191.
Ospina-Alvarez, A., Weidberg, N., Aiken, C., Navarrete, S., 2018. Larval transport in the upwelling ecosystem of central Chile: he effects of vertical migration, developmental time and coastal topography on recruitment. Prog. Oceanogr. 168. https://doi.org/10.1016/j.pocean.2018.09.016.
Pairaud, I.L., Gatti, J., Bensoussan, N., Verney, R., Garreau, P., 2011. Hydrology and circulation in a coastal area off Marseille: validation of a nested 3D model with observations. J. Mar. Syst. 88 (1), 20–33.
Parras-Berrocal, I.M., Waldman, R., Sevault, F., Somot, S., Gonzalez, N., Ahrens, B., et al., 2024. Response of the Mediterranean Sea surface circulation at various global warming levels: a multi-model approach. Geophys. Res. Lett. 51 (24), e2024GL111695.
Pascual, M., Rives, B., Schunter, C., Macpherson, E., 2017. Impact of life history traits on gene flow: a multispecies systematic review across oceanographic barriers in the Mediterranean Sea. PLoS One 12 (5), e0176419.
Pastor, F., Valiente, J.A., Khodayar, S., 2020. A warming Mediterranean: 38 years of increasing sea surface temperature. Remote Sens. 12 (17), 2687.
Peliz, A., Marchesiello, P., Dubert, J., Marta-Almeida, M., Roy, C., Queiroga, H., 2007. A study of crab larvae dispersal on the estern Iberian Shelf: physical processes. J. Mar. Syst. 68 (1), 215–236. https://doi.org/10.1016/j.jmarsys.2006.11.007.
Pinardi, N., Zavatarelli, M., Adani, M., Coppini, G., Fratianni, C., Oddo, P., et al., 2015. Mediterranean Sea large-scale low-frequency ocean variability and water mass formation rates from 1987 to 2007: a retrospective analysis. Prog. Oceanogr. 132, 318–332.
Pineda, J., Hare, J., Sponaugle, S., 2007. Larval transport and dispersal in the coastal ocean and consequences for population connectivity. Oceanography (Wash., D.C.) 20 (3), 22–39. https://doi.org/10.5670/oceanog.2007.27.
Pinot, J.-M., López-Jurado, J., Riera, M., 2002. The CANALES experiment (1996-1998). Interannual, seasonal, and mesoscale variability of the circulation in the Balearic Channels. Prog. Oceanogr. 55, 335–370. https://doi.org/10.1016/S0079-6611(02)00139-8.
Pipitone, C., Arculeo, M., 2003. The marine Crustacea Decapoda of Sicily (central Mediterranean Sea): a checklist with remarks on their distribution. Ital. J. Zool. 70 (1), 69–78.
Power, J., 1984. Advection, diffusion, and drift migrations of larval fish, 27-37. https://doi.org/10.1007/978-1-4613-2763-9_2.
Putman, N.F., He, R., 2013. Tracking the long-distance dispersal of marine organisms: sensitivity to ocean model resolution. J. R. Soc. Interface 10 (81), 20120979.
Rojas-Araos, F., Rojas-Hernández, N., Cornejo-Guzmán, S., Ernst, B., Dewitte, B., Parada, C., Veliz, D., 2024. Population genomic and biophysical modeling show different patterns of population connectivity in the spiny lobster *Jasus frontalis* inhabiting oceanic islands. Mar. Environ. Res. 193, 106253.
Rotllant, G., Aguzzi, J., Sarria, D., Gisbert, E., Sbragaglia, V., Río, J.D., Simeó, C.G., Mànuel, A., Molino, E., Costa, C., Sardà, F., 2015. Pilot acoustic tracking study on adult spiny lobsters (*Palinurus mauritanicus*) and spider crabs (*Maja squinado*) within an artificial reef. Hydrobiologia 742 (1), 27–38. https://doi.org/10.1007/s10750-014-1959-5.
Rotllant, G., Guerao, G., Gras, N., Estevez, A., 2014. Larval growth and biochemical composition of the protected Mediterranean spider crab *Maja squinado* (Brachyura, Majidae). Aquat. Biol. 20, 13–21. https://doi.org/10.3354/ab00540.
Šargač, Z., Giménez, L., González-Ortegón, E., Harzsch, S., Tremblay, N., Torres, G., 2022. Quantifying the portfolio of larval responses to salinity and temperature in a coastal-marine invertebrate: a cross population study along the European coast. Mar. Biol. 169 (6), 81. https://doi.org/10.1007/s00227-022-04062-7.
Sciascia, R., Guizien, K., Magaldi, M.G., 2022. Larval dispersal simulations and connectivity predictions for Mediterranean gorgonian species: sensitivity to flow representation and biological traits. ICES (Int. Counc. Explor. Sea) J. Mar. Sci. 79 (7), 2043–2054.
Ser-Giacomi, E., Jordá-Sánchez, G., Soto-Navarro, J., Thomsen, S., Mignot, J., Sevault, F., Rossi, V., 2020. Impact of climate change on surface stirring and transport in the Mediterranean Sea. Geophys. Res. Lett. 47 (22), e2020GL089941.
Ser-Giacomi, E., Legrand, T., Hernandez-Carrasco, I., Rossi, V., 2021. Explicit and implicit network connectivity: analytical formulation and application to transport processes. Phys. Rev. 103 (4), 042309.
Seytre, C., Vanderklift, M.A., Bodilis, P., Cottalorda, J.M., Gratiot, J., Francour, P., 2013. Assessment of commercial and recreational fishing effects on trophic interactions in the Cap Roux area (north-western Mediterranean). Aquat. Conserv. Mar. Freshw. Ecosyst. 23 (2), 189–201.
Simons, R.D., Siegel, D.A., Brown, K.S., 2013. Model sensitivity and robustness in the estimation of larval transport: a study of particle tracking parameters. Journal of Marine Systems 119, 19–29.
Sotelo, G., Morán, P., Posada, D., 2008. Genetic identification of the northeastern atlantic spiny spider crab as *Maja brachydactyla* (Balss, 1922). J. Crustac Biol. 28 (1), 76–81. https://doi.org/10.1651/07-2875R.1.
Steneck, R.S., 2006. Possible demographic consequences of intraspecific shelter competition among American lobsters. J. Crustac Biol. 26 (4), 628–638.
Swearer, S., Treml, E., Shima, J., 2019. A review of biophysical models of marine larval dispersal, 325-356. https://doi.org/10.1201/9780429026379-7.
Taebi, S., Lowe, R.J., Pattiaratchi, C.B., Ivey, G.N., Symonds, G., 2012. A numerical study of the dynamics of the wave-driven circulation within a fringing reef system. Ocean Dyn. 62, 585–602.

Torres, A., Dos Santos, A., Alemany, F., Massutí, E., 2013. Larval stages of crustacean species of interest for conservation and fishing exploitation in the western Mediterranean. Sci. Mar. 77, 149–160. https://doi.org/10.3989/scimar.03749.26D.
Vignoli, V., Caruso, T., Falciai, L., 2004. Decapoda Brachyura from monte argentario (Mediterranean Sea, central tyrrhenian). Crustaceana 77 (2), 177–186.
Yin, J., Overpeck, J., Peyser, C., Stouffer, R., 2018. Big jump of record warm global mean surface temperature in 2014–2016 related to unusually large oceanic heat releases. Geophys. Res. Lett. 45 (2), 1069–1078.
Zaimen, F., Ghodbani, T., Vermeren, H., 2021. L'activité de pêche artisanale au sud de la Méditerranée : Gouvernance, dynamique socio-économique et enjeux environnementaux dans le port algérien de Jijel (Boudis). VertigO-la revue électronique en sciences de l'environnement 21 (1).
Zakardjian, B.A., Runge, J.A., Plourde, S., Gratton, Y., 1999. A biophysical model of the interaction between vertical migration of crustacean zooplankton and circulation in the Lower St. Lawrence Estuary. Can. J. Fish. Aquat. Sci. 56 (12), 2420–2432. https://doi.org/10.1139/f99-095.

Further reading

Arakawa, A., 1977. Computational design of the basic dynamical processes of the UCLA general circulation model. Methods Comput. Phys: Adv. Res. Appl. 17, 337. General circulation models of the atmosphere.
Balss, H., Crustacea, V.I.I., 1922. Decapoda Brachyura (Oxyrhyncha und Brachyrhyncha) und geographische Übersicht über Crustacea Decapoda. Beitr. Kennt. Meeresfauna Westafr. 3, 71–110.
Steneck, R.S., 2006. Staying connected in a turbulent world. Science 311 (5760), 480–481.